National Transportation Safety Board

Office of Marine Safety
Washington, D.C. 20594-2000
December 13, 2016

ATTACHMENT 14 to the METEOROLOGY GROUP FACTUAL REPORT
DCA16MM001

Report providing estimates of wind and sea state parameters using state-of-the-art computer models provided by Environmental Monitoring Center at the National Centers for Environmental Prediction.

Submitted by: Mike Richards
NTSB, AS-30

U. S. Department of Commerce
National Oceanic and Atmospheric Administration
National Weather Service
National Center for Weather & Climate Prediction
5830 University Research Court
College Park, MD 20740

Technical Note

Estimating sea state and surface winds during Hurricane Joaquin using State-of-the-Art wave and hurricane models from the National Center for Environmental Prediction (NCEP)

Arun Chawla[‡]
Environmental Modeling Center
Marine Modeling and Analysis Branch

November 4, 2016

This report has been developed for the National Transportation Safety Board (NTSB)

[‡] e-mail: [redacted]@noaa.gov

This page is intentionally left blank.

This report is a study of the sea state and surface wind conditions during Hurricane Joaquin provided as a supplement to the National Transportation Safety Board (NTSB) to assist them in their investigation regarding the sinking of the Merchant Vessel El Faro. The study involved using high resolution hurricane and wave simulations to quantify the ocean conditions around the time of the accident. Numerical results were compared with observations to determine the skill of the simulations. Results from the study show that maximum wind speeds in the area around the time of accident exceeded 100 knots with waves reaching heights of between $7 - 10$ m and peak periods of $9 - 12$ s. Spectral results showed complex crossing sea patterns with swell and multiple wind sea components. Numerical data from the simulations have been provided to NTSB for further analysis. Data from this study has been used to study the development of extreme waves (separate report).

Acknowledgments. The author thanks Henrique Alves and Yung Chao from the Environmental Modeling Center (EMC) for helping with the initial set of runs. Hurricane model simulations and the underlying global wind fields came from the HWRF and Global data assimilation teams at EMC respectively. Thanks to Samuel Trahan from the HWRF group for help in processing the hurricane wind fields.

Contents

This page is intentionally left blank.

1 Introduction

Hurricane Joaquin was a powerful tropical storm that occurred in the Northwest Atlantic between late September and early October, 2015. The genesis of the storm was near the Bahamas on Sept. 26^{th}. Initially the storm moved towards the Bahamas, transitioning into a hurricane by Sept. 30^{th}. For the next two days it stayed in the region slowly strengthening into a Category 3 hurricane. By Oct. 3^{rd} it had turned around and started moving Northeastwards into the Atlantic Ocean, intensifying as it moved, before eventually dissipating out over the ocean around the middle of October. At its strongest the storm developed into a Category 4 hurricane.

One of the biggest casualties of the storm was the tragic sinking of the SS El Faro, a cargo ship, that was traveling from Florida to Puerto Rico. It lost its propulsion and was caught in the track of Hurricane Joaquin. The vessel with a crew of 33 sank at 1140 Hrs UTC on Oct. 1^{st1}. Search operations later carried out by the US Coast Guard, Air Force and Navy, revealed images and debris of the ship wreck.

As part of their investigation into the sinking of the El Faro, the National Transportation Safety Board (NTSB) has requested the National Oceanic and Atmospheric Administration (NOAA) to help them determine the sea state and wind conditions for the time period and region that correspond to the sinking of the El Faro. The Environment Modeling Center (EMC) at the National Center for Environmental Prediction (NCEP) has been tasked with this activity. EMC develops and maintains a suite of numerical models that are run every day to provide operational forecast guidance to the National Weather Service (NWS). These models include global atmospheric models for overall weather conditions, high resolution hurricane models to determine the development and propagation of hurricane winds and underlying ocean wave and circulation models to determine the ocean response to atmospheric forcings. Apart from the different advanced numerical engines, EMC also maintains a sophisticated suite of data assimilation algorithms that uses real time data from a vast network of satellite and in-situ observation system to develop accurate analysis fields that can drive these models.

For this study we have used archived wind fields from the atmospheric models to drive a high resolution wave model to determine the sea state under Hurricane Joaquin. The study has been limited to the time period when the storm was near the Bahamas, where the accident occurred. This report describes the results from that study. Section 2 describes the atmospheric and wave modeling systems that have been used. Section 3 a validation of the model results with available data is done to underline the skill in the simulations. Section 4 describes the atmospheric and sea conditions in the region around the time of the accident, and section 5

[1]This is the estimated time of the sinking at the time of the writing of the report

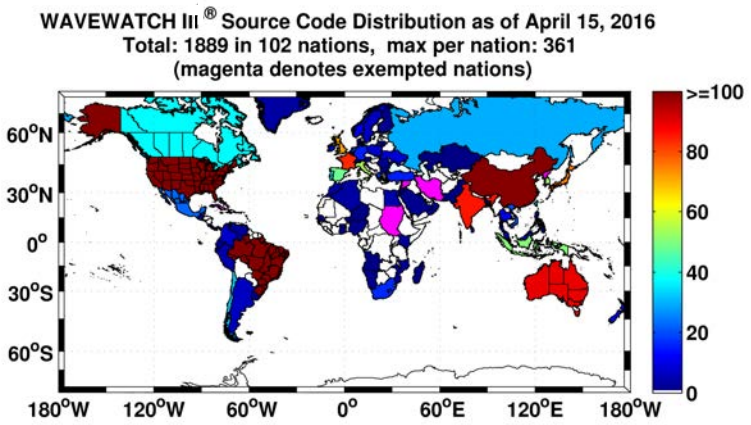

Figure 1: Distribution map of WAVEWATCH III® user community

lists the products that have been delivered to NTSB.

2 Modeling System

The purpose of this study is to develop as accurate an estimate of the sea state and winds in the region around the last known location of SS El Faro. To achieve this, EMC used the best available estimates for the winds from a hurricane wind model (see below) and used these winds to drive a third generation wave model using high resolution domains. The obtained fields were validated against available measurements of sea state and atmospheric conditions.

2.1 Wave Model

The wave model used at NCEP is a third generation wind wave model WAVEWATCH III® (Tolman, 2002, 2009, 2014). This wave model has been providing operational wave guidance to forecasters at the NWS since early 2000. It has been validated under several different conditions − Global evaluations : (Tolman et al., 2002; Chawla et al., 2013b,a); Hurricane conditions : (Tolman et al., 2005; Alves et al., 2014b); Great Lakes : (Alves et al., 2014a). The wave model is a State-Of-The-Art third generation wind wave model that has been developed at NCEP and downloaded for use in several countries (see Fig. 1). Apart from the United States, it is used in providing operational wave model guidance in UK (UK Met Office), Canada (Environment Canada), Australia (Bureau of Meteorology), France (Meteo France) and India (Indian National Center for Ocean Information Systems) to name a few centers.

The wave model characterizes the ocean surface as a two dimensional spectrum (in frequency and direction) and solves for the propagation, growth and

Table 1: WAVEWATCH III® grid particulars. All output data associated with a particular grid are identified by their grid labels.

Grid	Label	Latitude range	Longitude range	Resolution
Outer grid	natl_5m	$1.5°N : 45.5°N$	$98°W : 8°W$	$1/12°$
Inner grid	bhms_2m	$15°N : 30°N$	$84°W : 58°W$	$1/30°$

dissipation of wave energy as it moves in space and time. The model can account for many physical processes such as wave growth due to winds, wave - bottom interactions, wave - ice interactions, dissipation due to bottom friction and wave breaking etc. For this study interactions with currents and ice have been ignored. The main driving force for ocean waves are the wind fields at 10 m above Mean Sea Level (MSL). Section 2.3 outlines how the wind field over the wave domain was developed.

2.2 Domain Grid

The aim of this study is to determine the sea state around the site of the El Faro accident. Since the eye (center) of the hurricane passed through this region, very high resolution domains have been selected to accurately represent the rapidly changing sea state in the vicinity of the eye. WAVEWATCH III® can be run as a multi-nested system with two way nesting between the different nests. For this study we have have chosen two grids (see details in Table 1) − an outer domain (resolution $1/12°$) to capture the far field information and a higher resolution inner domain (resolution $1/30°$) to capture the detailed intensity of the hurricane. Figure 2 shows the extents of the two grids. Due to the two way nesting capability of the wave model, the sea state parameters are seamless across the boundaries of the two grids as seen by the plot of Significant Wave Height (Hs). For the rest of the report all the model output will be from the inner higher resolution nest which covers the region of the accident.

In spectral space the spectrum was discretized to have 40 components in frequency and 36 components in directional space. The frequency components range from $0.0285Hz - 1.17Hz$ with an increment factor set at 1.1 (frequency increments by 10%). This resolves waves with periods ranging from $0.85s - 35s$ and covers all the expected range of wind waves in the open ocean. In directional space the directional components correspond to a directional resolution of $10°$ and that defines the lower limit of our degree of uncertainty in wave directions.

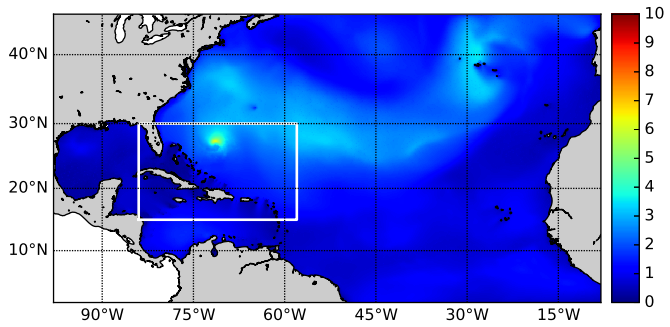

Figure 2: Domain for the wave simulations. The inner grid over the Bahamas is indicated by the white box. Grid particulars are given in Table 1. The colored values are Hs (in m) from the two grids.

2.3 Hurricane Model

The wind field at 10m above MSL is the critical forcing leading to the growth and propagation of ocean waves. As a result getting an accurate assessment of the hurricane winds is very important. In this study we use two sources of wind fields, both of which are created at NCEP – the Global Data Assimilation System (GDAS) and the Hurricane atmospheric model (HWRF). All the wind fields represented in this report (and used in driving the wave model) correspond to sustained winds (i.e. 10 minute averaged winds).

The GDAS system (Kanamitsu, 1989; Derber et al., 1991) is run 4 times a day (every 6 hours) and assimilates data from a global network of observations to develop a best guess of the atmospheric state that is then provided as initial conditions to run global forecast models. THE GDAS provides assimilated wind fields every hour out to 9 hours with each cycle. These data sets are archived on tapes at NCEP. Data from different GDAS cycle runs can be put together to provide a global wind field made up of best guess analysis for any given simulation period. Since this data set incorporates actual observations it is the closest that we have to ground truth. However the limitation of the GDAS is that the grid resolution ($\approx 1/2^{\circ}$) and the underlying physics (that are used to drive the data assimilation) is not adequate to resolve the strong wind intensities (wind speeds) under a hurricane.

The HWRF system (Tallapragada et al., 2015) is NCEP's hurricane model and is run 4 times a day (every 6 hours) just like the GDAS to provide numer-

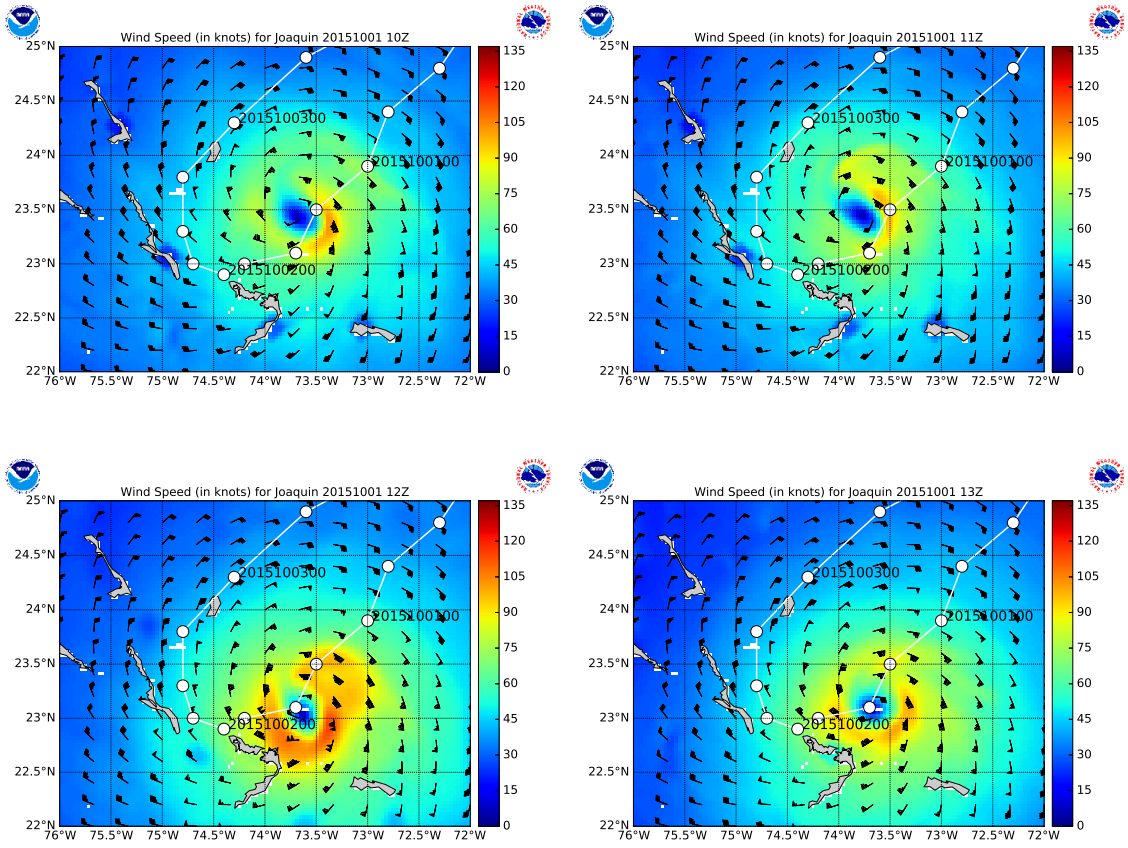

Figure 3: Snapshots of the wind speed (in knots) overlaid over the wind barbs. The best track for the hurricane eye (from the National Hurricane Center) is provided in white with the time stamp reported in YYYYMMDDHH format. All times are in UTC

ical guidance for hurricane forecasting. This system is only run when there are hurricanes. The 4 cycles correspond to 0, 6, 12 and 18 hours (in UTC). For each cycle there is a nowcast state (hour 0) that determines the initial condition by assimilating all the available measurements into the model (using algorithms similar to the ones used in the GDAS but at much higher resolutions), and a forecast state (hours 1 through 126) that provides the atmospheric state on an hourly basis out into the future. Like any forecast modeling system, the skill of the model decreases with increasing forecast hours. The HWRF system consists of 3 nests (18km outer nest resolution, 6km middle nest resolution and a 2 km inner nest resolution) with the outer most coarsest nest getting its boundary conditions from the Global atmospheric model (GFS) and the inner most high resolution nest moving with the hurricane to properly resolve the eye of the hurricane. Apart from the higher resolution nested domains, the HWRF modeling system differs from the GDAS in the physics packages used which have been tuned for high intensity hurricane conditions.

For this study we use the first 6 hours of HWRF wind fields (Hour 0 - 5) from each cycle to build a wind field that covers the entire run period of our simulation. The HWRF winds are interpolated on to the wave model grids with the highest resolution winds getting the first priority. However, since waves tend to propagate outside the area of influence of winds as swells, the wave model domain used in this study is much bigger than the HWRF domain (see Fig. 2). Outside the HWRF domain we use the wind fields from the GDAS to get the underlying global back ground wind field. A blending scheme is used to blend the GDAS and HWRF winds to provide a seamless wind field over the entire wave model domain.

Figure 3 shows the wind field around the area of the accident for different time stamps. The formation of the eye of the hurricane can be clearly seen, and in the simulations the modeled eye tracks the observed location of the storm at different time stamps (also shown). The wind speeds in the simulations reach over 100 knots which matches with observations made during the hurricane (more on this in the validation section). One thing to note is the shift in the hurricane winds between the snapshot at 11Z[2] and 12Z. This is because at the 12Z snapshot the modeling system is using the nowcast data (Hour 0 from the 12Z cycle) which includes assimilated data and thus provides a more realistic representation of the hurricane. This occurs 4 times a day (at the 0,6,12 and 18Z time snaps) and thus at these time stamps the confidence in the model results are higher. This point should be kept in mind when trying to estimate the conditions around the time of the accident.

[2]In this report we use Z (Zulu time) and UTC (Coordinated Universal Time) interchangeably. They both refer to the same time

3 Validation

For validation we rely on the buoy data (available from the National Data Buoy Center - NDBC) and altimeter tracks that lie close to the path of the hurricane as well as the storm intensity (maximum velocity) as has been reported by the National Hurricane Center (NHC). Figure 4 shows the location of the buoys used in the validation study along with the path of the hurricane. The color bar indicates the recorded central pressure at the eye of the storm, with lower pressures indicative of an intensifying hurricane. Just like the model runs, the hurricane track particulars (location of storm center, maximum winds, central pressure storm radii etc.) are reported every 6 hours on the 0, 6, 12 and 18Z cycles by NHC. The genesis of the storm starts with the 6Z cycle on the Sept. 25^{th}. After the initial propagation to the North, the storm turns back towards the Bahamas and starts intensifying as indicated by the drop in central pressure. The storm reaches hurricane status some time after the 6Z cycle on Sept. 30^{th} (central pressure drops below 980 millibars) as it moves towards the Bahamas. The storm continues to intensify as it moves slowly towards the Bahamas archipelago with the central pressure continuing to drop. The hurricane turns around by the 12Z cycle on Oct. 2^{nd} and then proceeds to rapidly move out North East into the Atlantic Ocean. All together the storm remains in the area of interest (region where the accident occurred) between Sept. 30^{th} and Oct. 4^{th}.

For the purposes of this study we are interested in simulating the conditions between Sept. 30^{th} and Oct. 4^{th} in a region from $76°W - 72°W$ and $22°N - 25°N$. However to properly set up the wave conditions we start our simulations from the beginning of Sept. 20^{th} all the way to Oct. 4^{th} over the wave domain grids defined in Fig 2.

Figure 5 compares the wind intensities (maximum wind speed) from our simulations with the observations reported by NHC. While there is some scatter, the development of the storm is picked up very well from the simulations. The storm starts intensifying sometimes after 6Z on Sept. 30^{th} as it moves towards the Bahamas (see Fig 4 for corresponding hurricane track) matching increase in wind speeds with drop in central pressure. The storm becomes a Category 3 level storm (intensity > 95 knots) by 0Z on Oct. 1^{st} and a Category 4 level storm (intensity > 115 knots) around 18Z on the same day. The storm then continues to maintain this level of intensity as it turns around on Oct. 2^{nd} and subsequently starts traveling North East out into the Atlantic Ocean. Some of the scatter in the comparisons is due to the sampling differences (intensity data are reported every 6 hours while the model provides hourly estimates). The impact of data assimilation can be clearly seen as the model moves towards data at the 4 cycles per day (which correspond to the reporting time for the hurricane tracks as well). In general the model is accurate to within ± 10 knots of the data, with occasionally deviating to ≈ 20 knots (e.g. 12 Z on Oct. 3^{rd}).

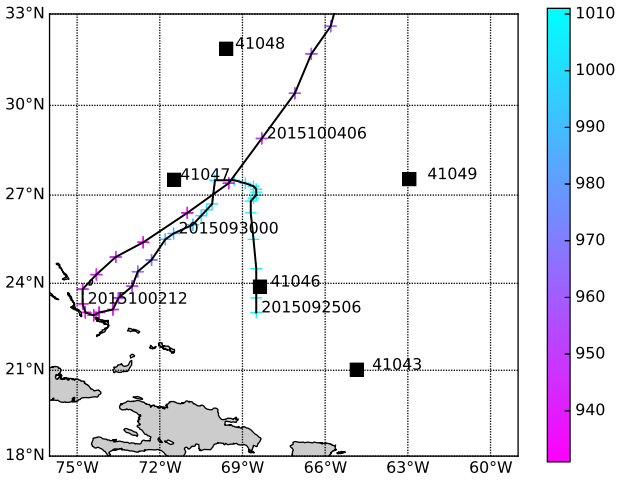

Figure 4: Buoy locations with the path of the hurricane. The colored bar indicates the central pressure recorded at the eye of the storm. The location of the eye of the storm is indicated by the '+' sign, and is reported every 6 hours (data from the National Hurricane Center) from the genesis of the storm. The color indicates the recorded central pressure at the eye. A few dates for the location of the storm center are provide in YYYYMMDDHH format. All times are in UTC

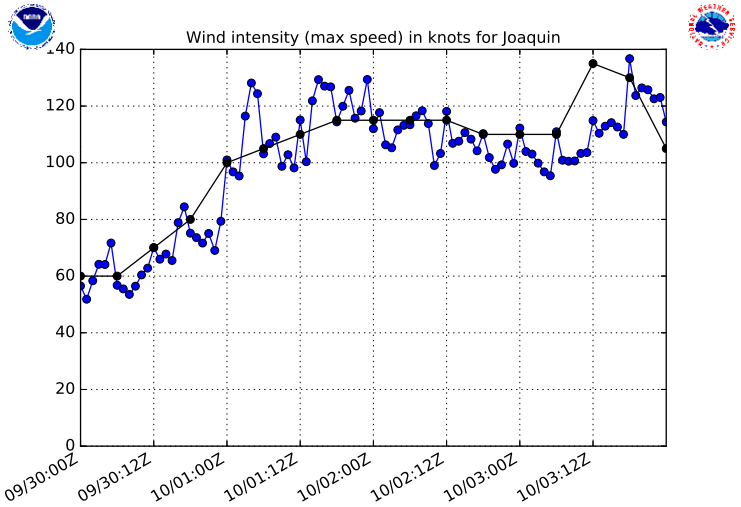

Figure 5: Hurricane intensity (maximum speed in knots) as a function of time. 'Black' data reported by the National Hurricane Center; 'Blue' model results obtained from the inner grid. Time is in MM/DD:HH format. All times are in UTC

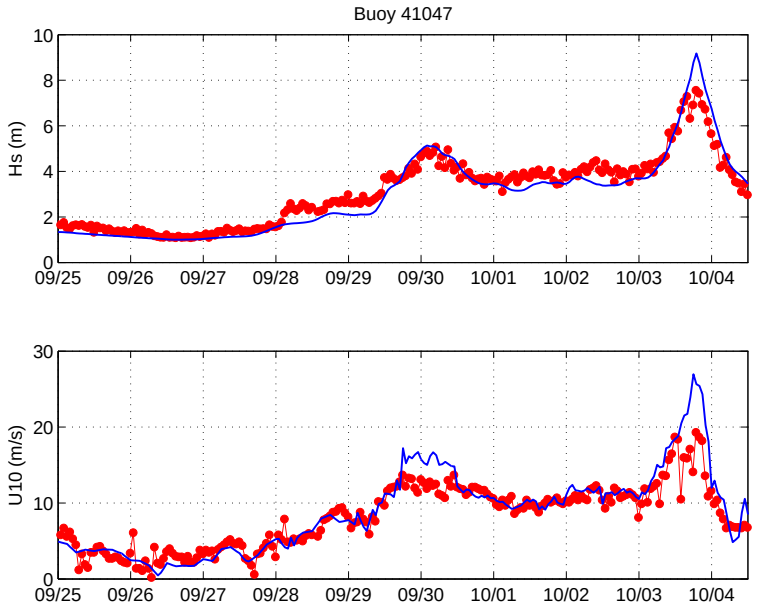

Figure 6: Comparison at buoy 41047 for Hs (in m) and U10 (in m/s). Data in 'red' ; Model in 'blue'. Time is in MM/DD format. All times are in UTC

Comparisons between in-situ buoys and observations for Hs and the 10 m above MSL wind speed (U10) are shown in Figs $6 - 10$. Buoys 41047, 41048 and 41049 lie either along the path of the storm or close to it after it intensifies into a hurricane. The increase in wave energy and corresponding wind speeds as the storm passes by the buoys are well represented. Though for buoy 41047 some part of the eye of the hurricane passes over the buoy in the data but not in the model. At buoy 41046, the model indicates that some signature of the hurricane is observed when the storm turns towards the Bahamas (Oct. 1^{st}) and when it turns back out and leaves the region (Oct. 4^{th}). This is not seen in the data, though there seems to be some small signature of the storm in the wave heights towards the end of the signal.

Apart from the total significant wave height, spectral comparisons of the sea state were also done between the model and the data (Figs. $11 - 15$). Once again, apart from buoy 41046 which shows signatures of the hurricane in the model but not in the data, at the other buoys the sea states are well represented. For example, as the storm approaches buoy 41047 (Fig. 11) between Oct. 3^{rd} and 4^{th} both model and data clearly show the arrival of leading swells first followed by the slower wind seas. The corresponding frequencies of these systems are well reproduced. In general the model is doing a very good job of representing the sea state.

Comparisons closer to the hurricane were also possible using derived mea-

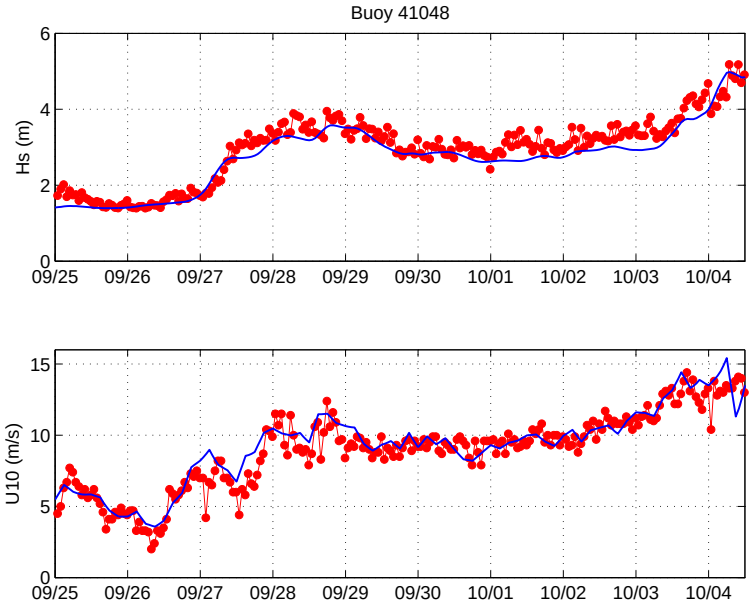

Figure 7: Comparison at buoy 41048 for Hs (in m) and U10 (in m/s). Data in 'red' ; Model in 'blue'. Time is in MM/DD format. All times are in UTC

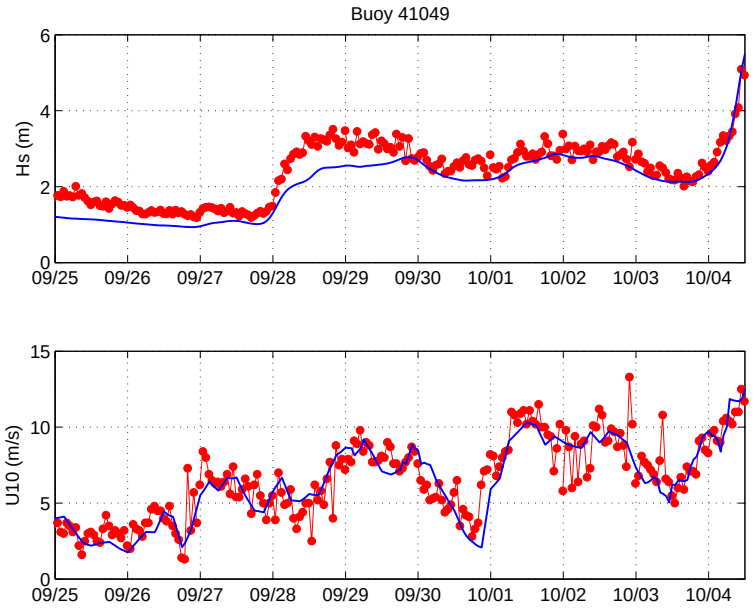

Figure 8: Comparison at buoy 41049 Hs (in m) and U10 (in m/s). Data in 'red' ; Model in 'blue'. Time is in MM/DD format. All times are in UTC

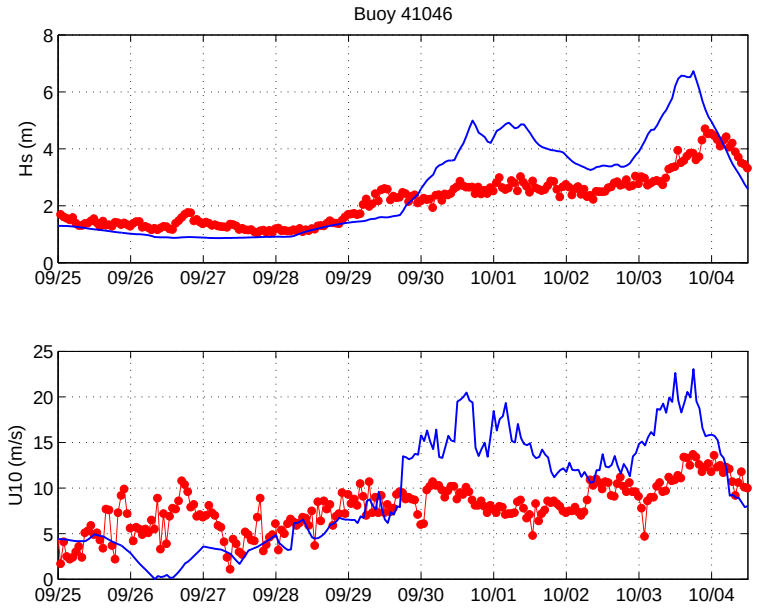

Figure 9: Comparison at buoy 41046 for Hs (in m) and U10 (in m/s). Data in 'red' ; Model in 'blue'. Time is in MM/DD format. All times are in UTC

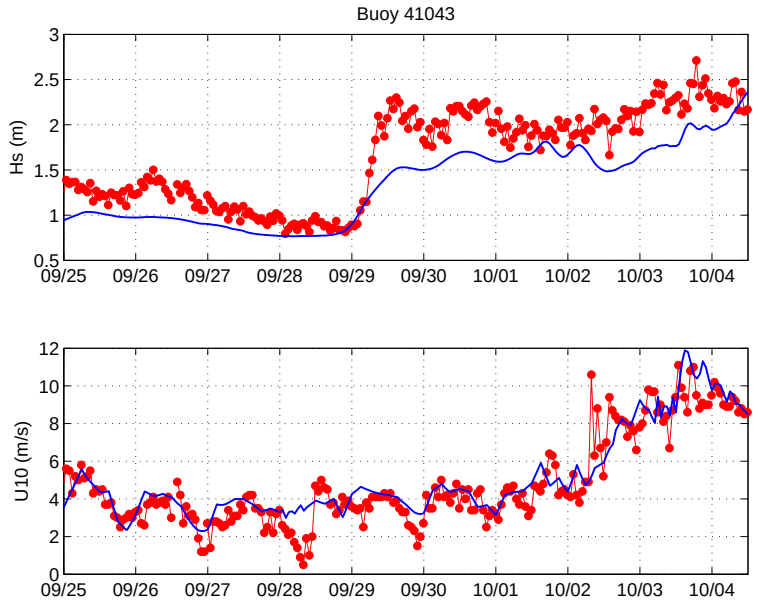

Figure 10: Comparison at buoy 41043 for Hs (in m) and U10 (in m/s). Data in 'red' ; Model in 'blue'. Time is in MM/DD format. All times are in UTC

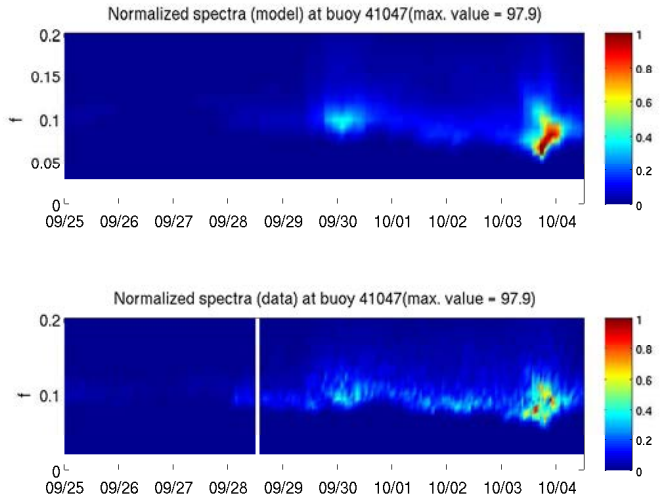

Figure 11: Spectral comparison as a function of time and frequency at buoy 41047. Model top panel. Spectra have been normalized by the maximum observed spectral value over the comparison period. Time is in MM/DD format. All times are in UTC

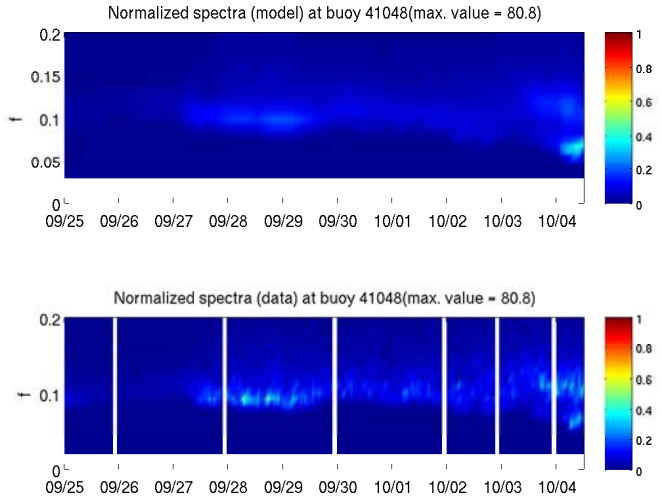

Figure 12: Spectral comparison as a function of time and frequency at buoy 41048. Model top panel. Spectra have been normalized by the maximum observed spectral value over the comparison period. Time is in MM/DD format. All times are in UTC

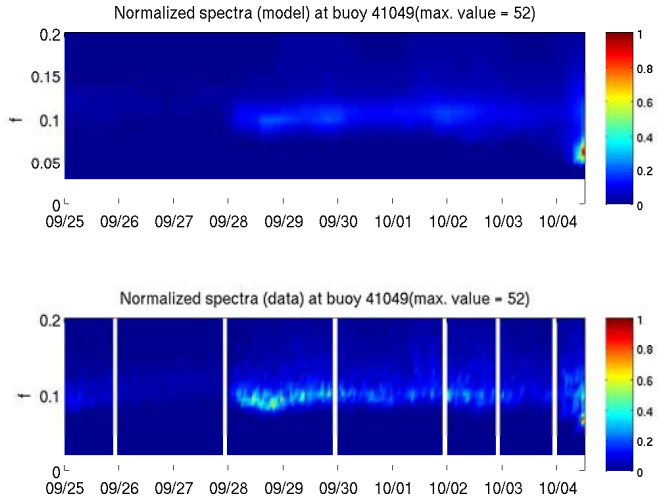

Figure 13: Spectral comparison as a function of time and frequency at buoy 41049. Model top panel. Spectra have been normalized by the maximum observed spectral value over the comparison period. Time is in MM/DD format. All times are in UTC

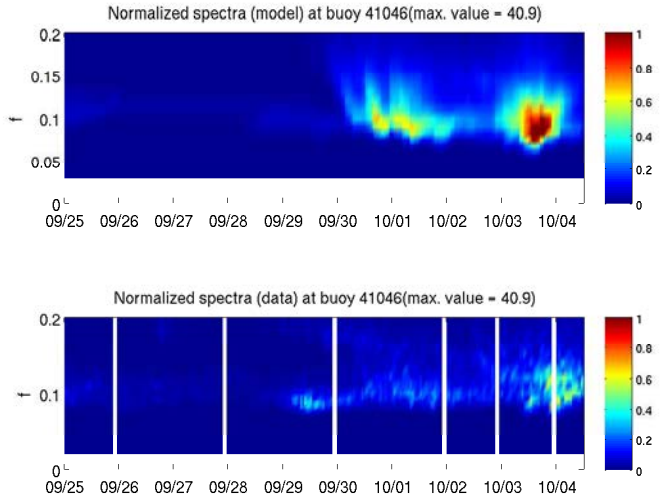

Figure 14: Spectral comparison as a function of time and frequency at buoy 41046. Model top panel. Spectra have been normalized by the maximum observed spectral value over the comparison period. Time is in MM/DD format. All times are in UTC

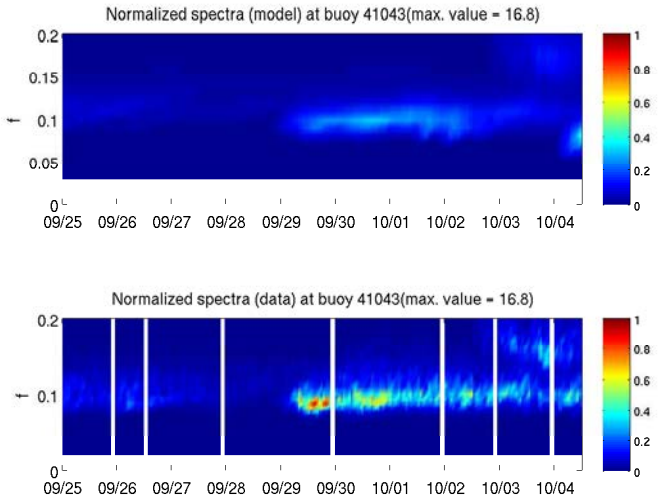

Figure 15: Spectral comparison as a function of time and frequency at buoy 41043. Model top panel. Spectra have been normalized by the maximum observed spectral value over the comparison period. Time is in MM/DD format. All times are in UTC

surements from satellite data. The Jason-2 altimeter track passed close to the hurricane at 1400 UTC on Oct 1^{st} (Fig. 16)[3]. Comparison between the model and altimeter derived Hs and U10 have been done by interpolating the model data along the altimeter track. The hurricane signature including the width of the storm are captured well by the model results. Some scatter in satellite data are expected as the track passes close to land.

[3]the track crosses the domain between 1409 and 1415 UTC on Oct 1^{st}

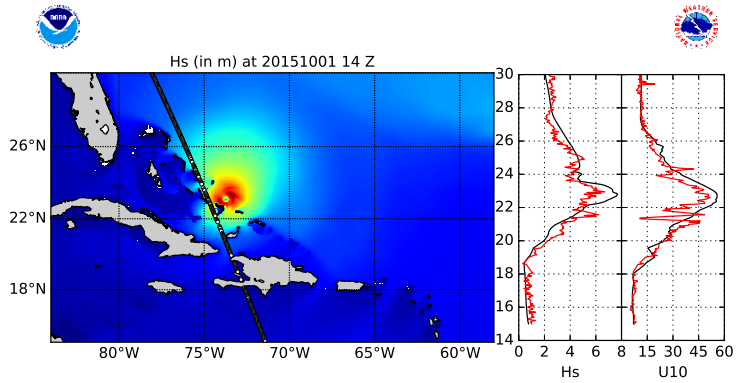

Figure 16: Comparison of model and data Hs and U10 using altimeter data from the Jason-2 satellite. Left panel shows the altimeter track along with model Hs map at the time of the crossing. Right two panels compare the Hs (in m) and U10 (in knots) between model and data along the track as a function of latitude (y axis). 'Black' Hs from model ; 'Red' Hs from altimeter. Model data has been interpolated to the altimeter track in time and space.

4 Sea state and atmospheric conditions at accident site

The El Faro is suspected of sinking during the morning hours of Oct 1^{st} (estimated sinking time 1140 hours UTC). It's last known position was approximately $73.90°W$ and $23.38°N$. Figures $17 - 19$ shows the hourly snapshots of the wind speeds in this area for Oct 1^{st}. The hurricane intensifies as it approaches this area, with wind speeds exceeding 100 knots by 1200 UTC and even greater than 120 knots by late afternoon.

The corresponding sea states (Significant wave height and peak period) are shown in Figures $20 - 25$. The wave heights are in the range of $7 - 10$ m and becoming greater than 12 m later in the afternoon, with the peak period ranging between 10 - 12 sec. The peak period is ≈ 10 s near the eye of the storm (area of active generation) and transitions to $12 - 15$ s swells away from the storm center.

Apart from bulk spectral properties, detailed spectral data was also output at specific locations. Since there was some ambiguity about the accident site[4], spectral data was output at several locations around the region to provide a picture of the complex sea state. Table 2 provides a list of all the output points. Hourly spectral data plots corresponding to these points are shown in Appendix A. Figure 26 shows the spectral data as a function of frequency and direction in polar coordinates around the time of accident at one such location. Frequency increments in radial direction with lower frequencies (swell fields) closer to the center. Wind vectors are represented by the size (wind speed magnitude) and direction of the arrow in the center of the plots. Angular direction represents the direction in which wave energy is propagating with North being at the top of the circle and East being to the right. Colors indicate spectral magnitudes with blue (red) corresponding to low (high) spectral values. For example at 8Z on Oct 1^{st}, the plot indicates wave energy propagating to the South with broad directional spreading. The sea state typically consists of a wind sea component that is moving with the winds and a swell component that is in a different direction from the winds (in this case moving towards the North West). At other locations, the turning winds yield more than two components, indicating complex crossing seas (see the plots in Appendix A for details).

[4]At the time of the writing of this report a preliminary sinking location of $73.90°W$ and $23.38°N$ was provided by NTSB to EMC

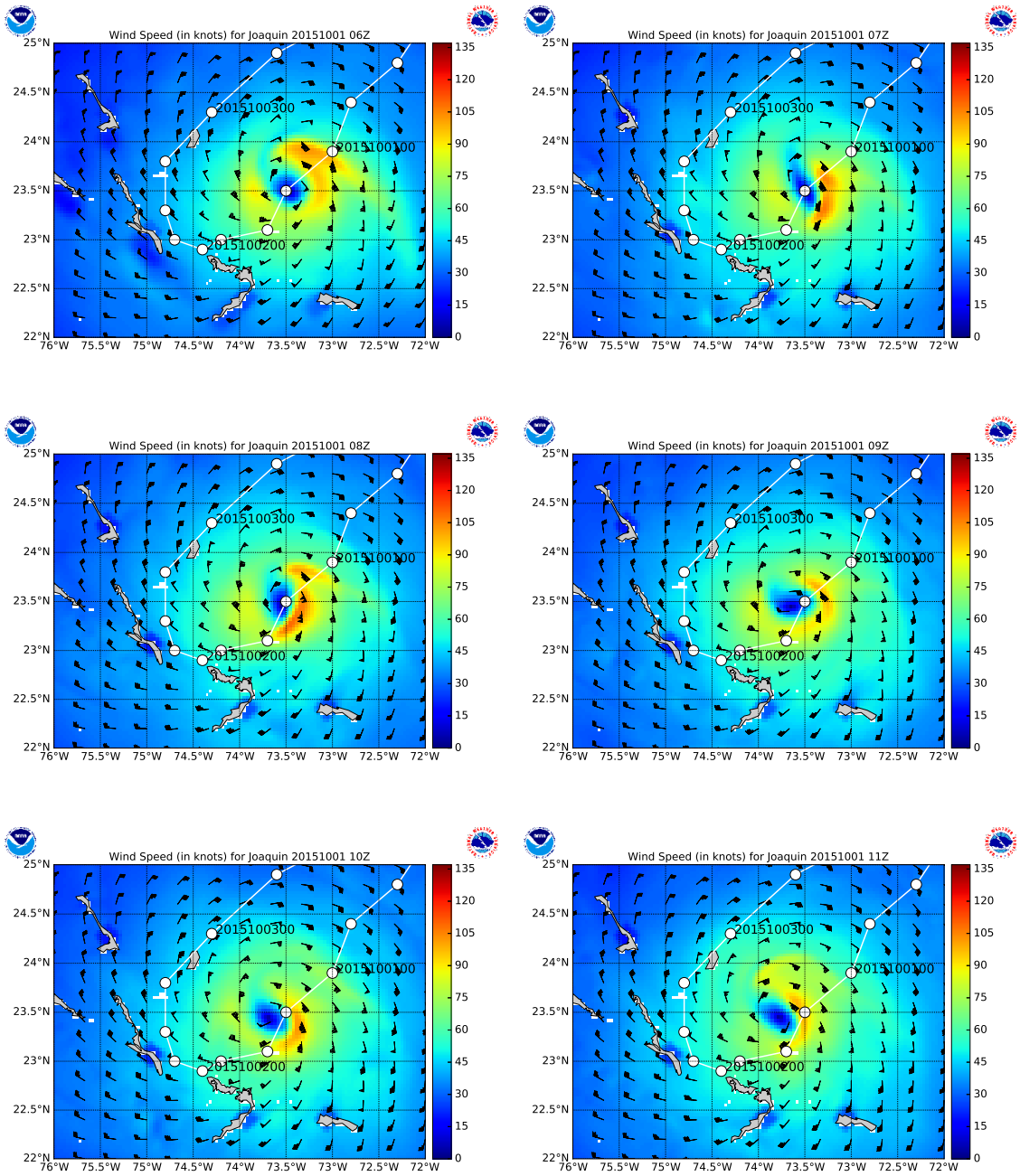

Figure 17: Snapshots of the wind speed (in m/s) between 6Z and 11Z on Oct 1^{st}. Hurricane track and wind barbs also shown (See Fig. 3 for details)

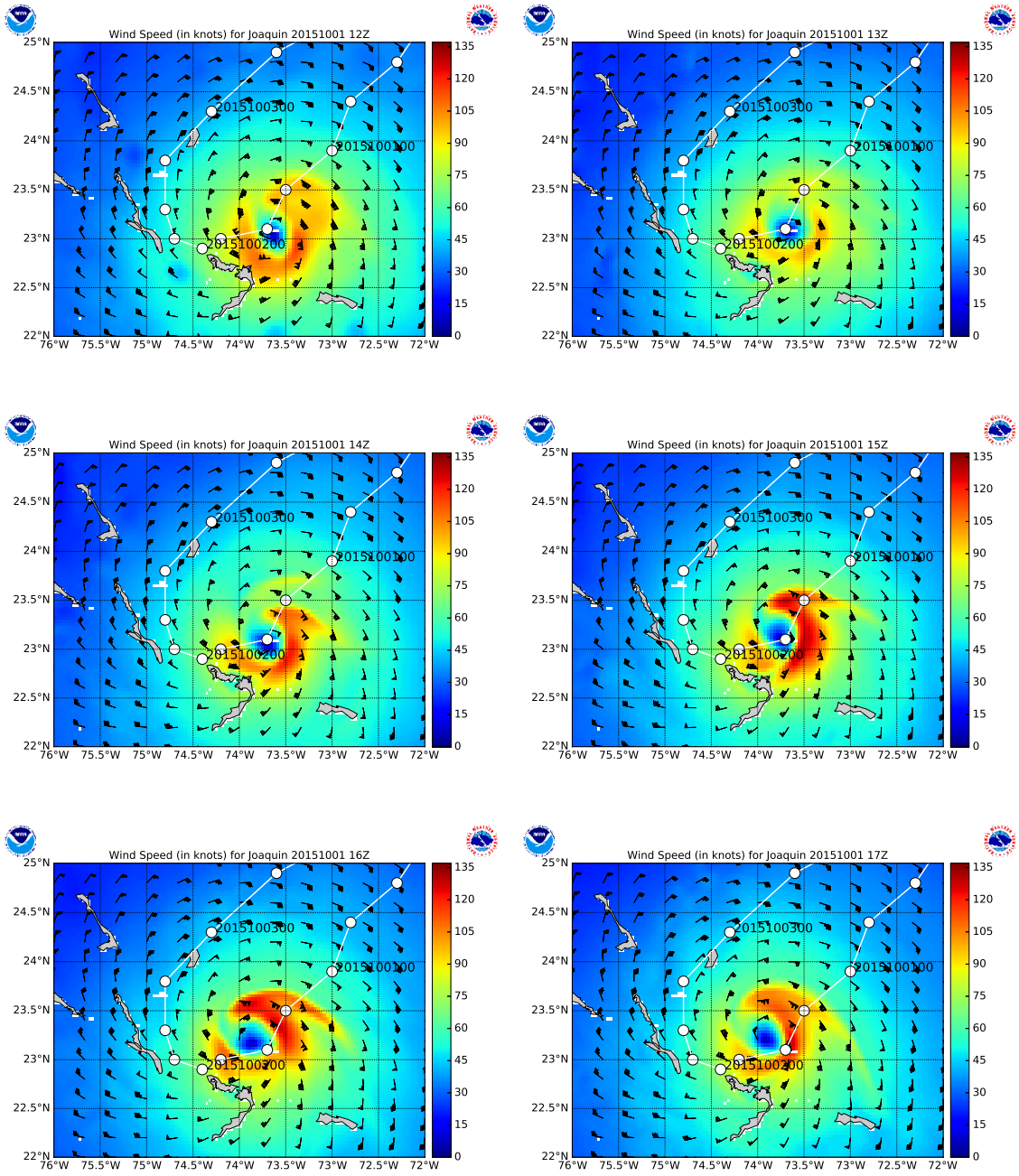

Figure 18: Same as Figure 17 but for hours 12Z through 17Z

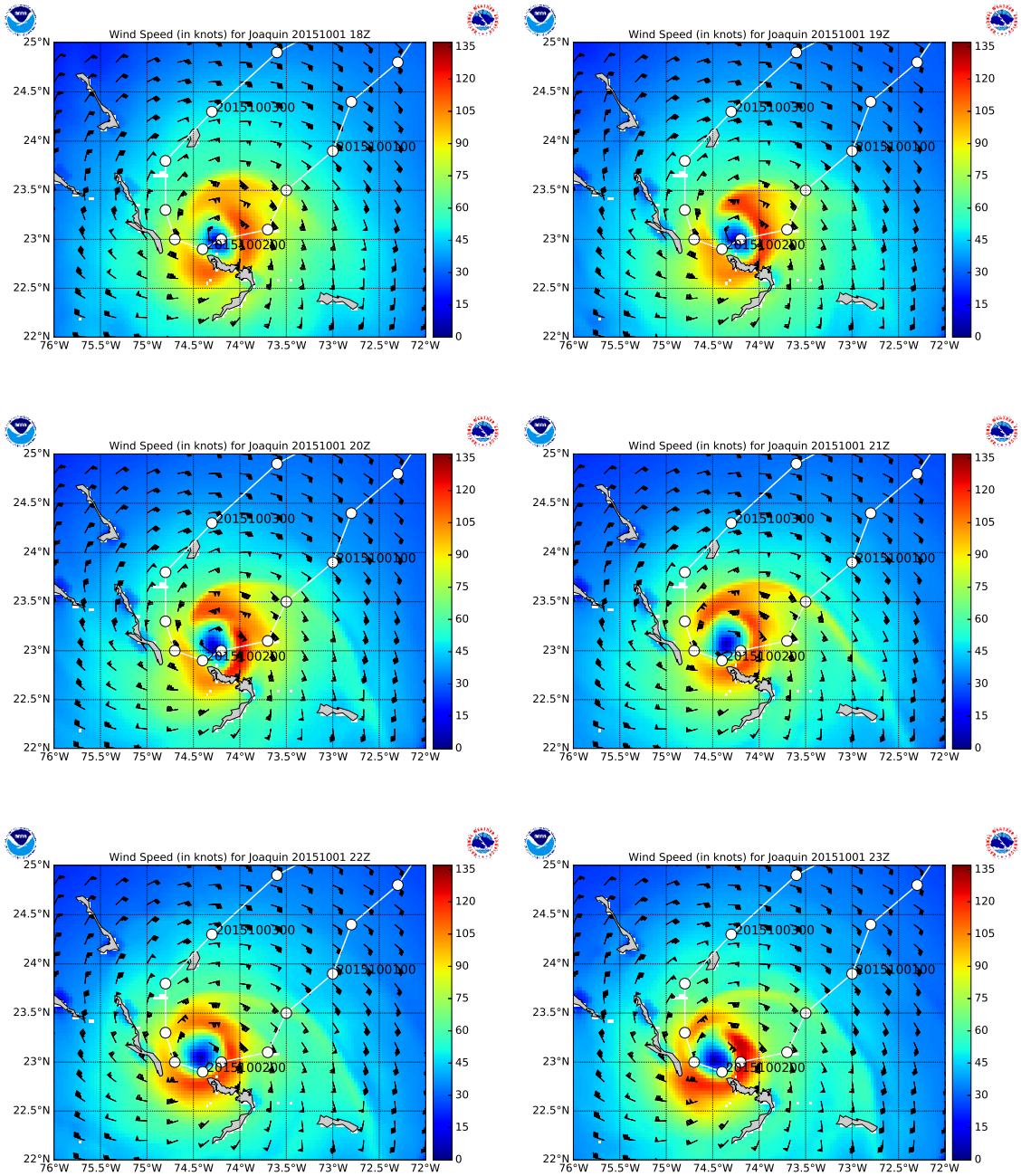

Figure 19: Same as Figure 17 but for hours 18Z through 23Z

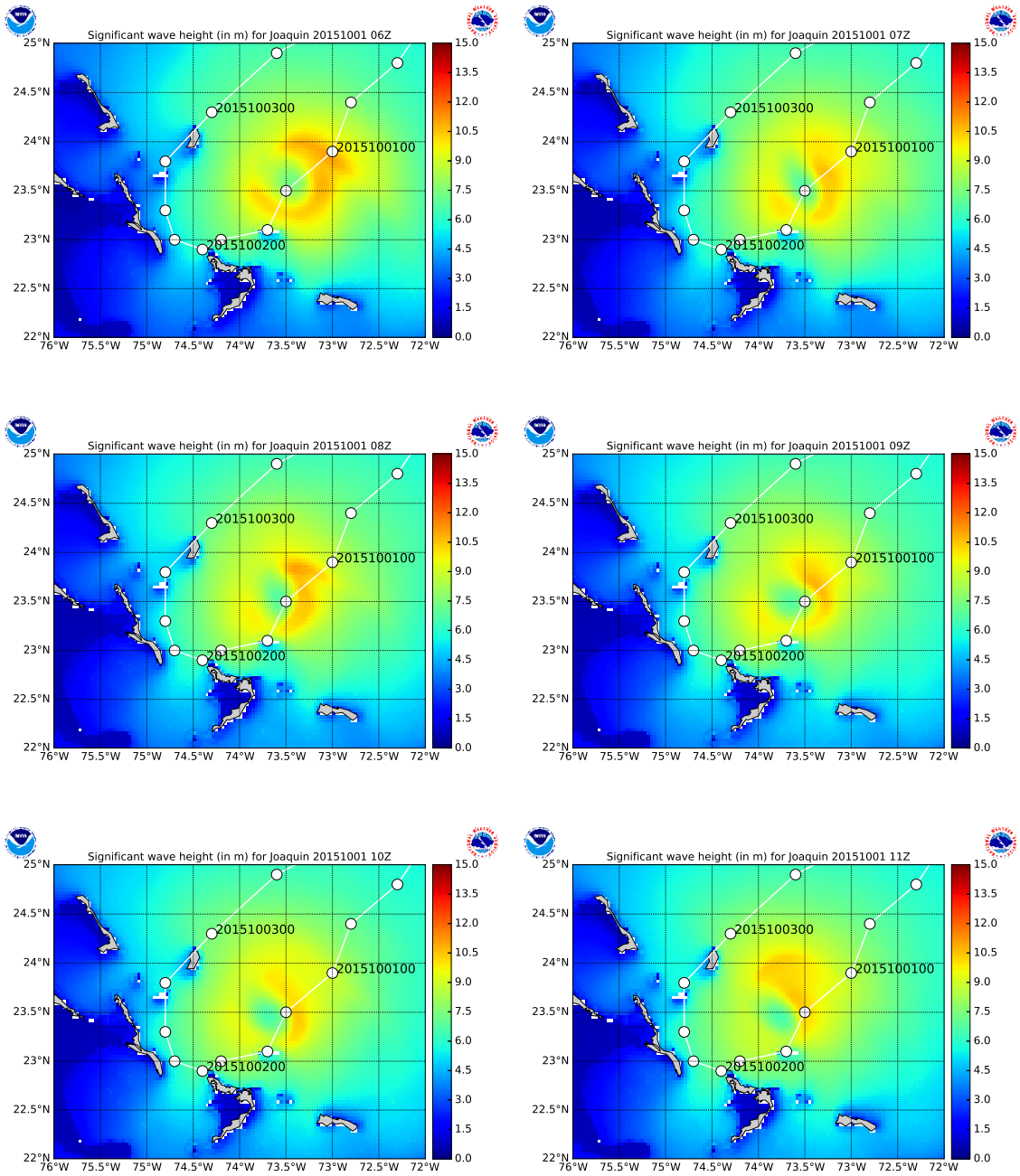

Figure 20: Snapshots of Significant wave height(in m) between 6Z and 11Z on Oct. 1^{st}. Hurricane track also shown (See Fig. 3 for details)

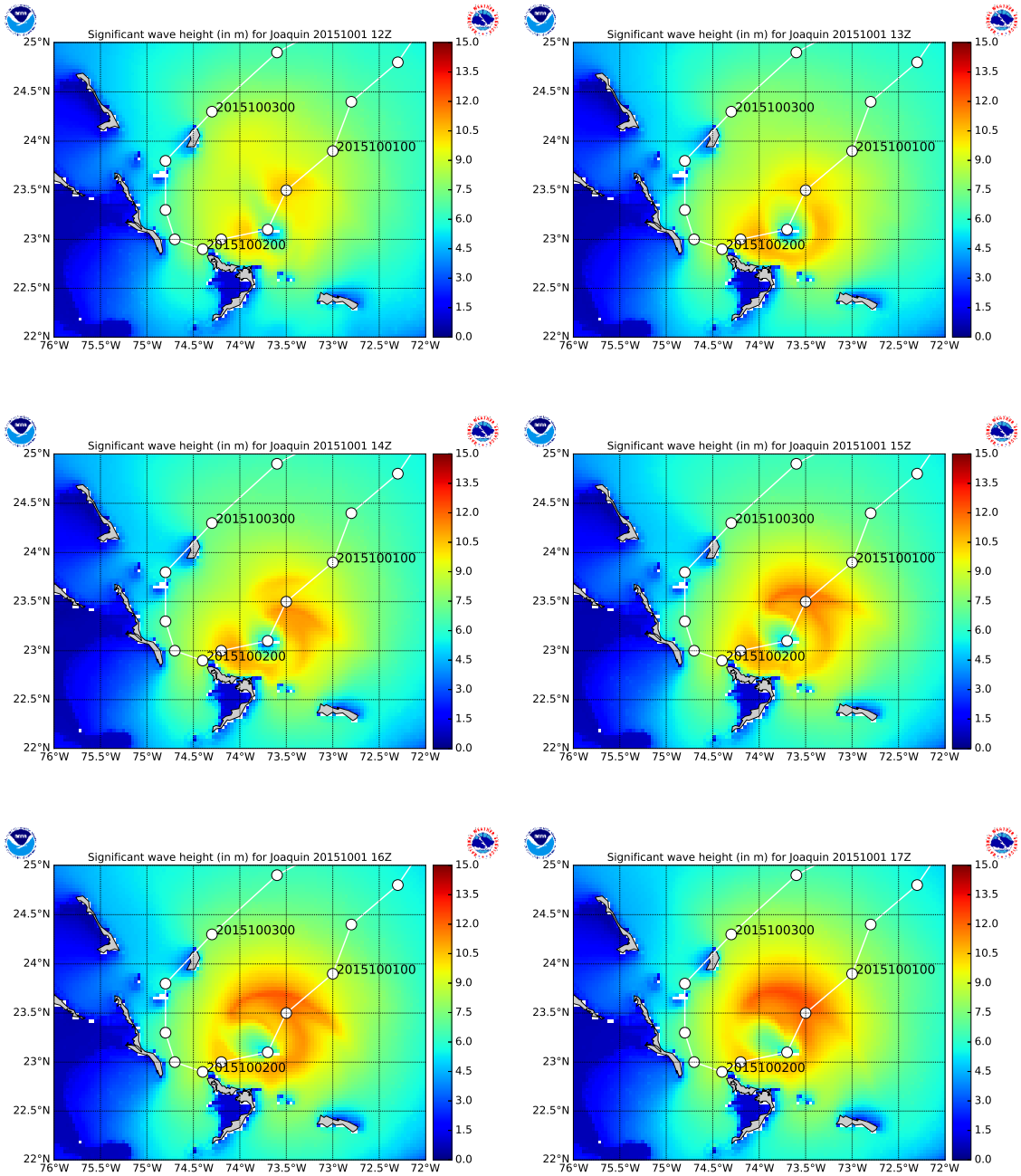

Figure 21: Same as Figure 20 but for hours 12Z through 17Z

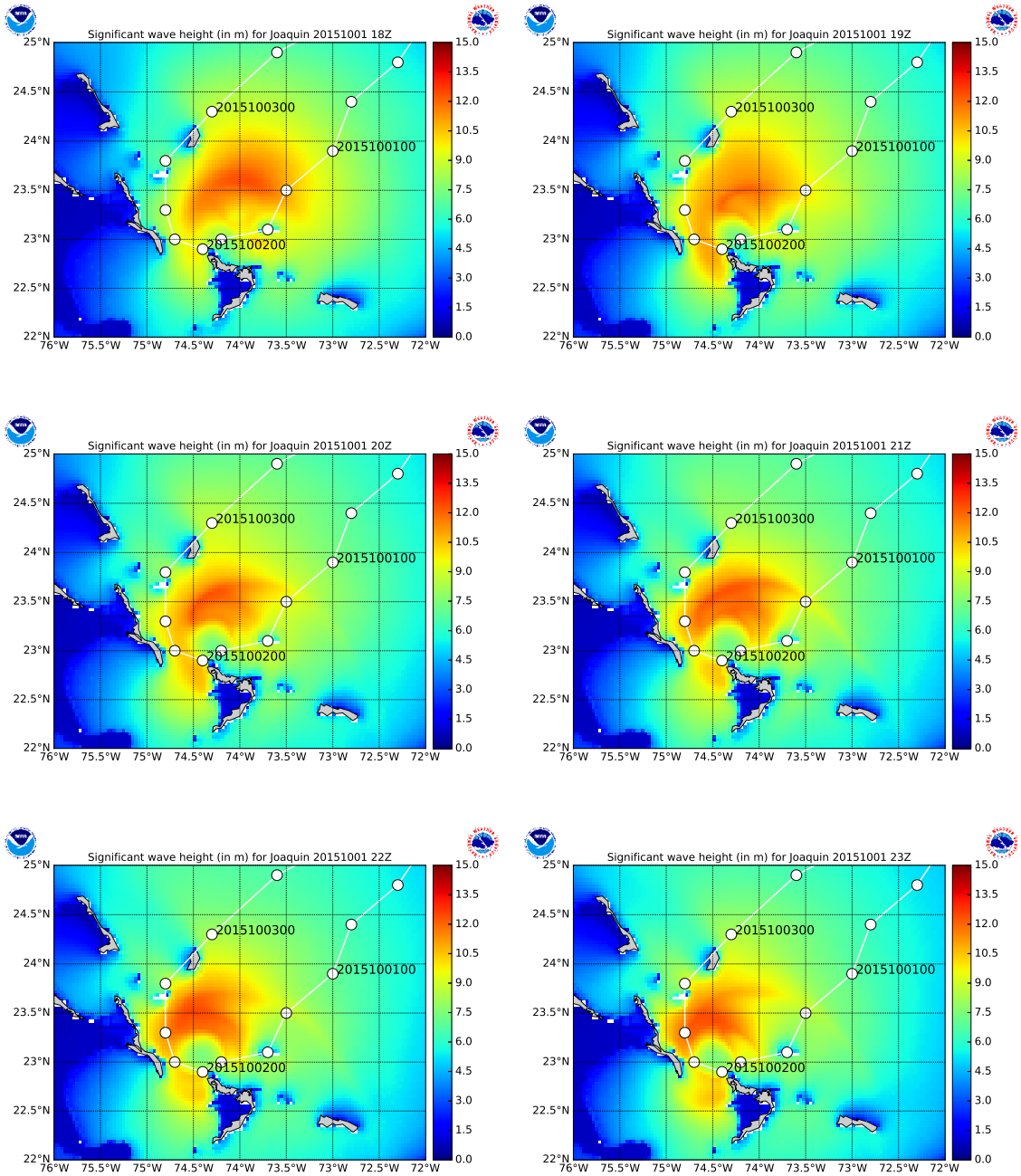

Figure 22: Same as Figure 20 but for hours 18Z through 23Z

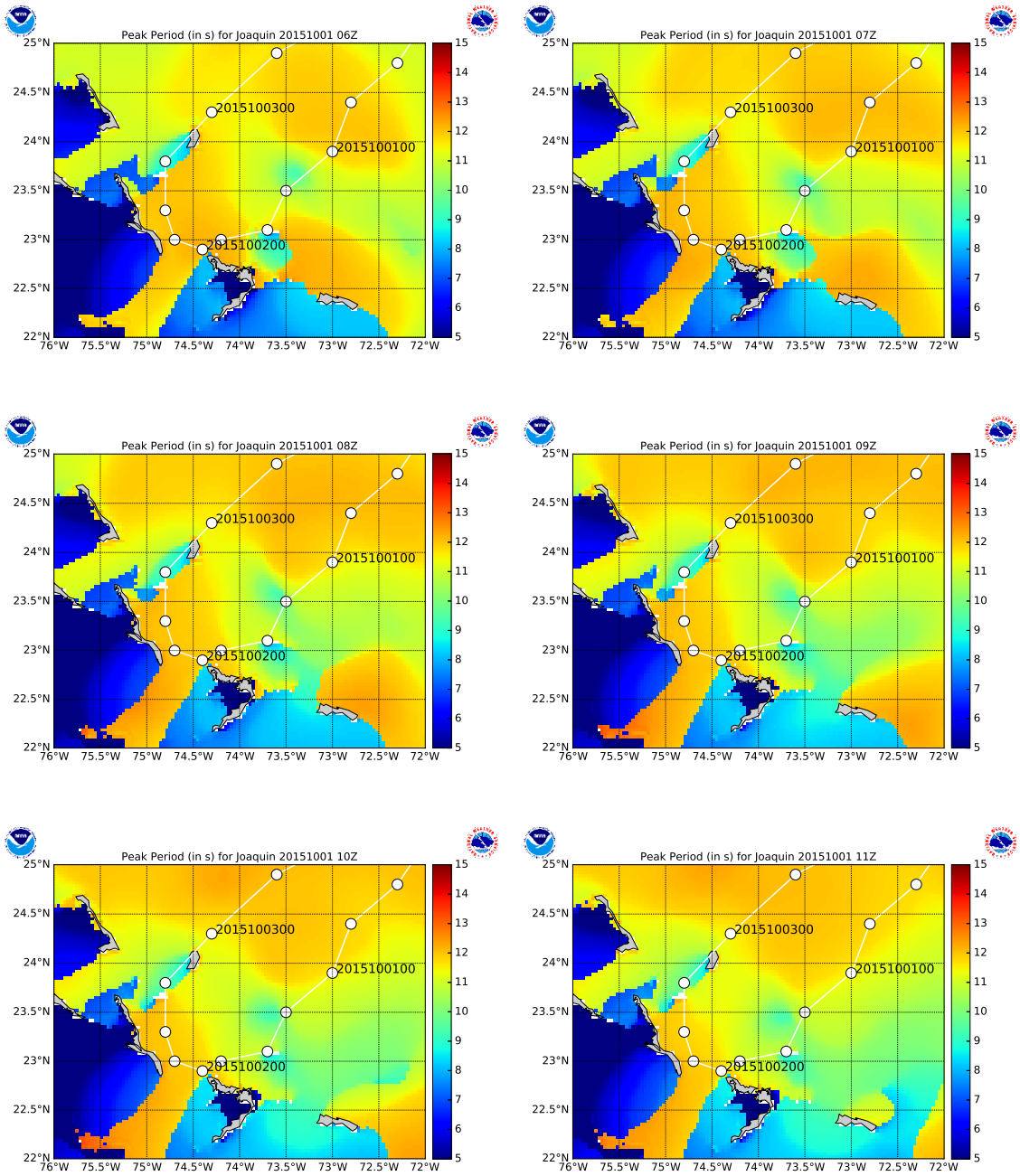

Figure 23: Snapshots of the Peak Period (in s) between 6Z and 11Z on Oct. 1^{st}. Hurricane track also shown (See Fig. 3 for details)

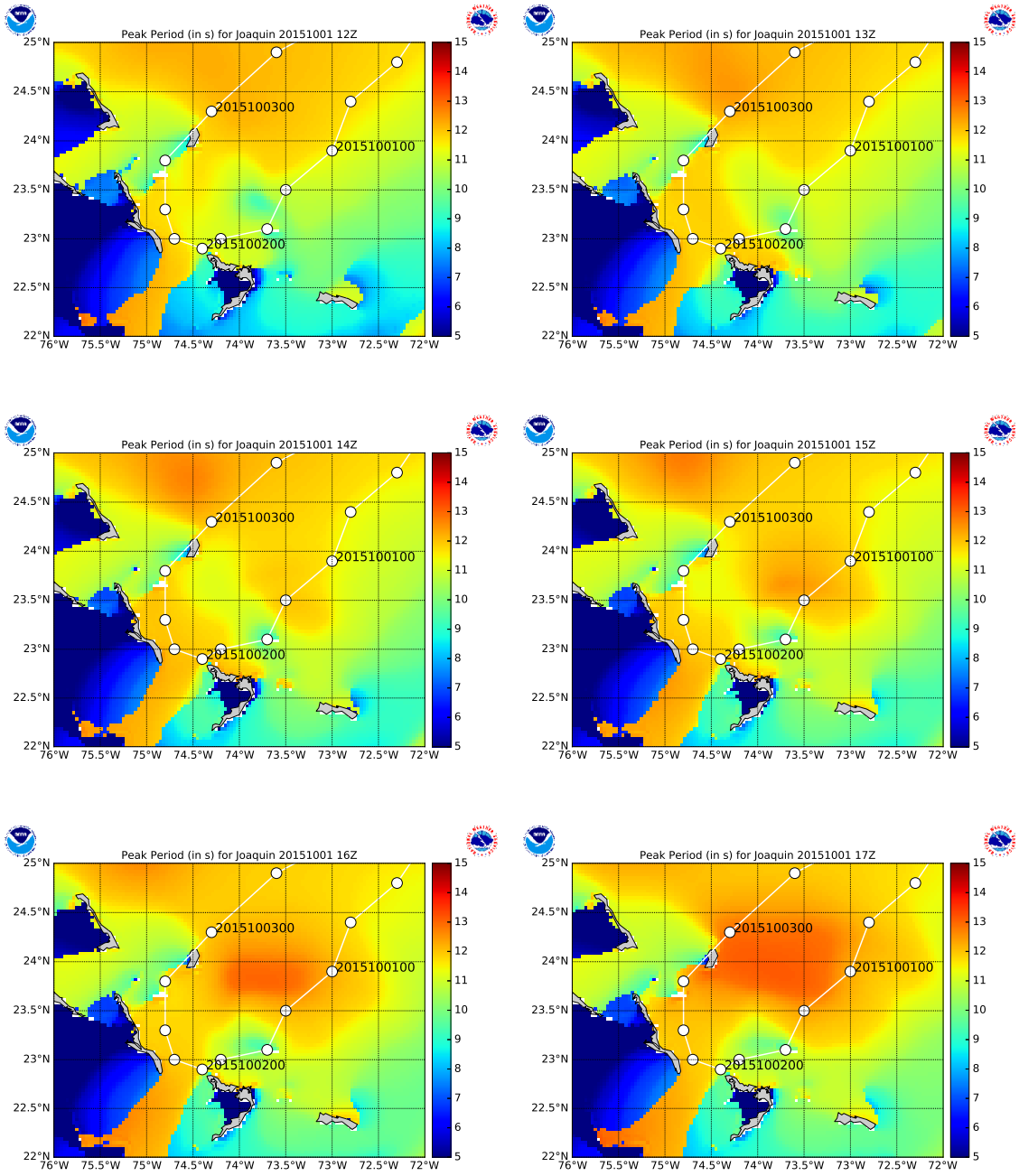

Figure 24: Same as Figure 23 but for hours 12Z through 17Z

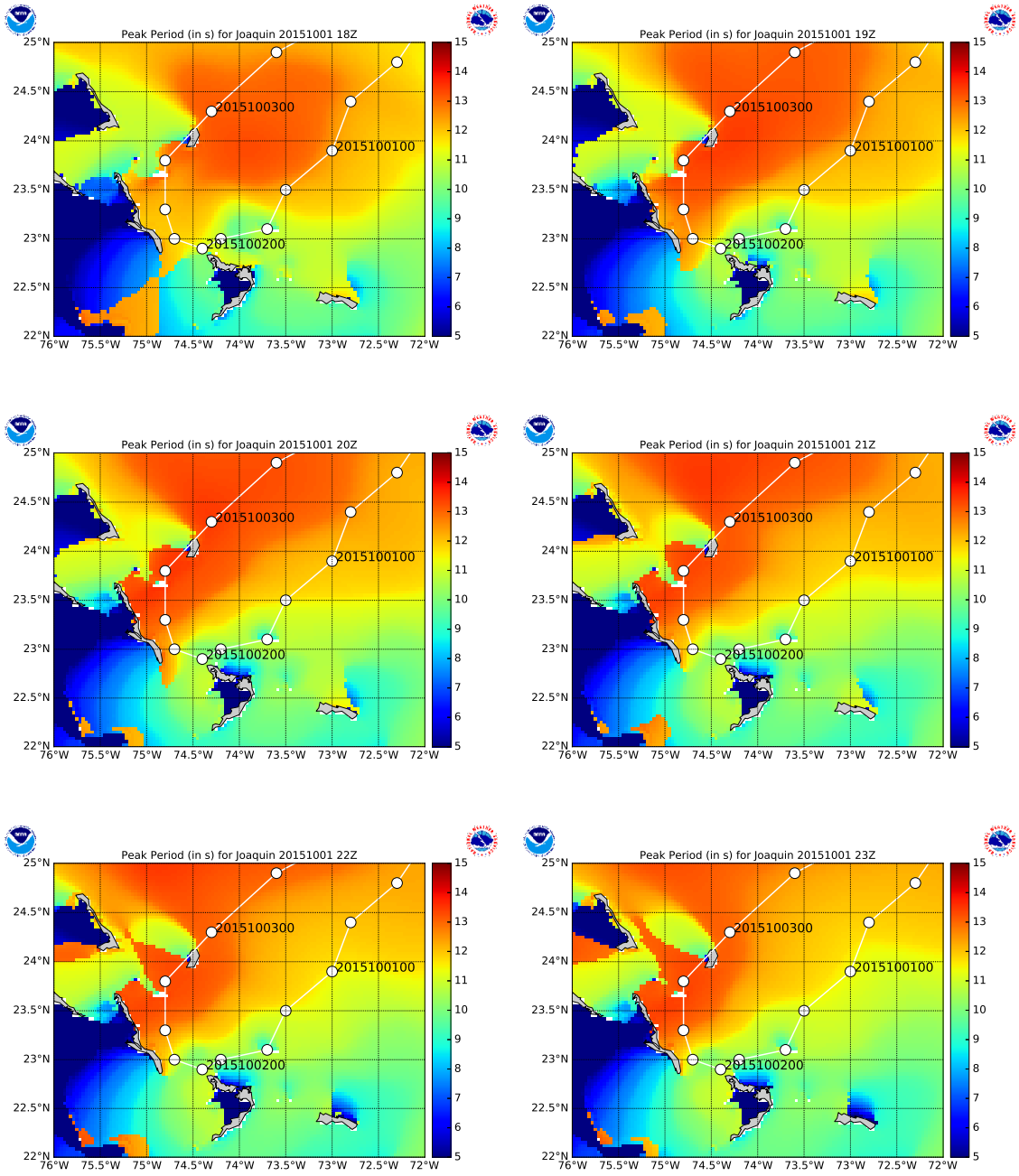

Figure 25: Same as Figure 23 but for hours 18Z through 23Z

5 Delivered Products

All output from the simulations are available on an hourly time interval from Sept. 30^{th} to Oct. 4^{th}. The output products include bulk spectral properties on grid layout and detailed spectral information at predetermined specific point locations. Unless otherwise specified all units are MKS.

5.1 Grib Files

Field output are produced on the two different model grid layouts (Table 1) and are produced in GRIB2 format. The file naming convention is as follows

[GRID ID].grb2

where

GRID ID Is the grid label for a specific grid (see Table 1).

The different fields stored in the grib2 files are identified by their grib2 labels. These are (in order of storage)

WIND : Wind speed in m/s (at 10 m above MSL)

WDIR : Wind direction in degrees, using nautical convention (direction from which the wind is blowing in compass notation, i.e. 0° is from the North, 90° is from the East and so on)

UGRD : Zonal component (East - West) of wind speed in m/s. Positive value corresponds to Eastward flow

VGRD : Meridional component (North - South) of wind speed in m/s. Positive value corresponds to Northward flow

HTSGW : Overall (integrated over the full spectrum) Significant wave height in m

PERPW : Peak period in s. Corresponds to the frequency of the spectrum with maximum energy

DIRPW : Average direction at the peak period in degrees. Direction notation follows the convention used for winds

WVHGT : Significant wave height for the wind sea component in m. The wind sea component is defined as the part of the spectrum that is directly under the action of the winds

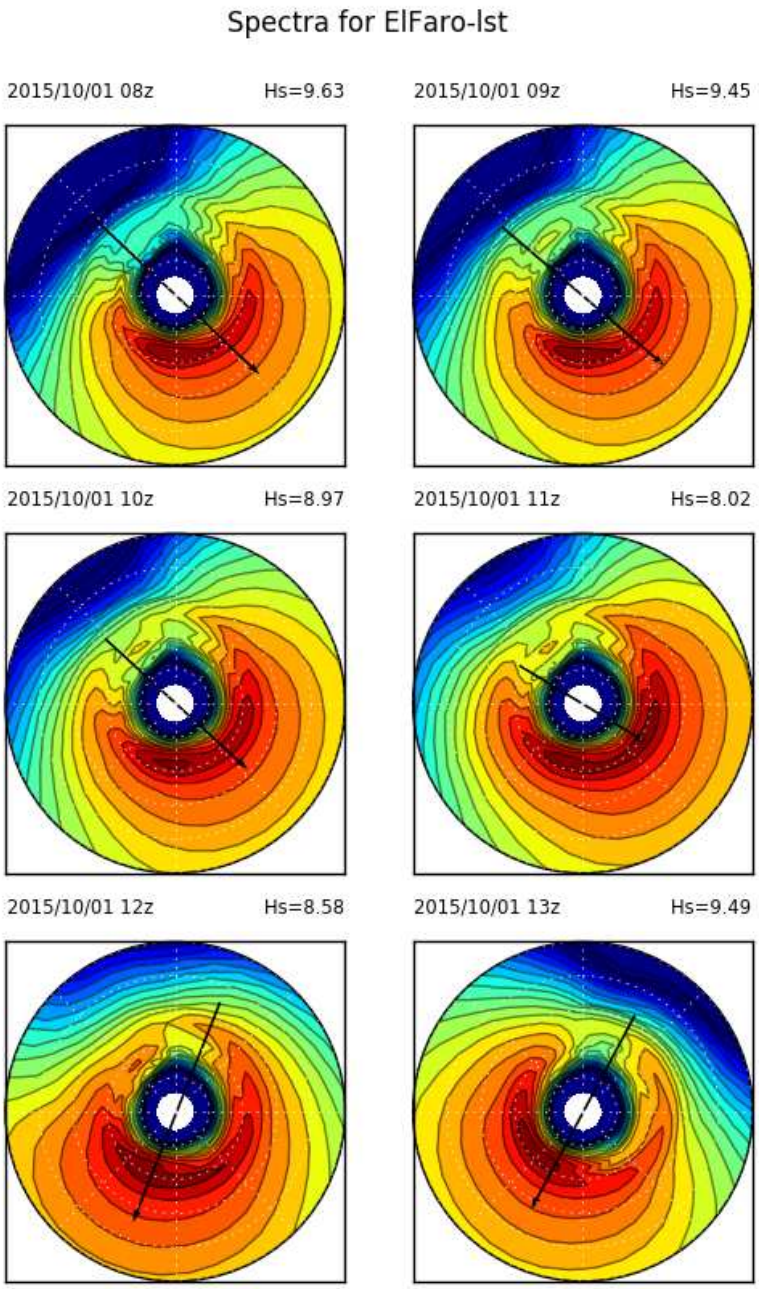

Figure 26: Spectral plot in polar coordinates as a function of frequency (radial) and direction (angular) for point ElFaro-lst (location is $-73.92°W$ and $23.38°N$; from Table 2)

SWELL : Significant wave height for the swell component in m. There are up to 5 swell components reported with the swell fields being ranked by wave heights. If no swell component exists at a particular point then the field at that point is marked as undefined

WVPER : Similar to WVHGT but for peak period following the notation of PERPW

SWPER : Similar to SWELL but for peak period following the notation of PERPW

WVDIR : Similar to WVHGT but for direction following the notation of DIRPW

SWDIR : Similar to SWELL but for direction following the notation of DIRPW

All data are in grid layout and contain values on ocean points with land points being undefined (exception is wind data that is defined over land and water). For wind seas and swell spectral parameters, data is defined only where they exist. For example, near the center of the storm which is an area of active wave generation, there are no swell fields only wind seas, and thus here the swell fields are marked as undefined.

There is no frequency cut off that is used to separate wind seas from swells. Instead a partitioning algorithm is used to separate the spectrum into different wave components and a wave age type criterion is used to determine if a particular component is under the direct influence of winds (phase speed is less than wind speed) and can hence be classified as wind sea, or is no longer being directly influenced by the wind (phase speed greater than the wind speed) and can hence be classified as a swell field. More details can be found in Tolman (2014).

5.2 Point Output

There are 94 output points where the full 2D spectral information (frequency - direction) on an hourly increment are stored in ASCII format. These output points are a mix of points at locations of buoys from the National Data Buoy Center (NDBC) some of which have been used in validating the model results (Section 3), and others are points of interest in the investigation into the El Faro accident. Table 2 lists the coordinates for the output points together with the unique identifiers used to distinguish them.

The format for these spectral files are

```
<Text string> <Nfr> <Nd> <Np> <Text String>
<fr> (for all frequency bins)
<dir> (for all direction bins)
<yymmdd> <hhmmss>
```

```
<Text string> <lat> <lon> <d> <uabs> <udir> <cabs> <cdir>
<E(fr,dir)> (for all frequencies and directions)
repeat for all times
.
.
.
```

where

Nfr,Nd,Np are the number of frequencies, directions and points respectively. Since a separate file is being generated for each point, Np is set at 1.

fr,dir are the discretized frequency (in Hz) and direction (in radians) bins. Direction is in oceanographic convention.

lat,lon,d are the latitude, longitude and water depth (in m) at the point

E(fr,dir) are the wave spectra in m^2/Hz.

An example Matlab script for reading spectral data files is given in Appendix B.

Table 2: Point output locations with coordinates in longitudes and latitudes and identifier strings. The longitude coordinates range from -180 to 180 (with the negative values corresponding to W). The latitude coordinates range from -90 to 90 (with the negative values corresponding to S). Point output was generated at locations corresponding to buoys from NDBC (IDs starting with 4*) as well as locations of interest to the investigation (IDs starting with ElFaro*)

Lon	Lat	ID	Lon	Lat	ID	Lon	Lat	ID
-73.8	23.4	ElFaro-01	-73.8	23.6	ElFaro-33	-65.01	20.99	41043
-73.6	23.4	ElFaro-02	-76.428	26.309	ElFaro-34	-70.99	24.00	41046
-73.4	23.4	ElFaro-03	-76.195	26.064	ElFaro-35	-71.49	27.47	41047
-73.2	23.4	ElFaro-04	-75.969	25.829	ElFaro-36	-69.65	31.98	41048
-73.0	23.4	ElFaro-05	-75.758	25.572	ElFaro-37	-63.00	27.50	41049
-72.8	23.4	ElFaro-06	-73.878	23.42	ElFaro-sas	-58.69	21.65	41044
-72.6	23.4	ElFaro-07	-73.92	23.38	ElFaro-lst	-77.71	34.14	41110
-72.4	23.4	ElFaro-08	-53.08	14.55	41040	-81.29	30.72	41112
-72.2	23.4	ElFaro-09	-46.00	14.53	41041	-80.53	28.40	41113
-72.0	23.4	ElFaro-10	-57.90	15.90	41100	-80.22	27.55	41114
-72.0	23.6	ElFaro-11	-56.20	14.60	41101	-75.78	36.91	44099
-72.0	23.8	ElFaro-12	-72.66	34.68	41001	-75.59	36.26	44100
-72.0	24.0	ElFaro-13	-75.36	32.32	41002	-70.43	38.48	44004
-72.0	24.2	ElFaro-14	-79.09	32.50	41004	-69.16	43.19	44005
-72.0	24.4	ElFaro-15	-80.87	31.40	41008	-69.43	40.50	44008
-72.0	24.6	ElFaro-16	-66.58	41.11	44011	-74.70	38.46	44009
-72.0	24.8	ElFaro-17	-62.00	42.26	44137	-74.84	36.61	44014
-72.0	25.0	ElFaro-18	-53.62	44.26	44138	-72.10	40.70	44017
-72.2	25.0	ElFaro-19	-57.08	44.26	44139	-71.01	41.38	44070
-72.6	25.0	ElFaro-20	-51.74	43.75	44140	-69.29	41.26	44018
-72.8	25.0	ElFaro-21	-58.00	43.00	44141	-73.70	40.37	44065
-73.0	25.0	ElFaro-22	-64.02	42.50	44142	-72.60	39.58	44066
-73.2	25.0	ElFaro-23	-64.01	42.50	44150	-65.93	42.31	44024
-73.4	25.0	ElFaro-24	-80.17	28.50	41009	-73.17	40.25	44025
-73.6	25.0	ElFaro-25	-78.47	28.95	41010	-73.12	40.59	44094
-73.8	25.0	ElFaro-26	-80.60	30.00	41012	-71.13	40.97	44097
-73.8	24.8	ElFaro-27	-77.74	33.44	41013	-70.17	42.80	44098
-73.8	24.6	ElFaro-28	-75.40	35.01	41025	-67.31	44.27	44027
-73.8	24.4	ElFaro-29	-77.28	34.48	41035	-67.88	43.49	44037
-73.8	24.2	ElFaro-30	-76.95	34.21	41036	-66.55	43.62	44038
-73.8	24.0	ElFaro-31	-77.36	33.99	41037			
-73.8	23.8	ElFaro-32	-77.72	34.14	41038			

6 Conclusion

Hurricane Joaquin was a Category 4 storm that was active in the Northern Atlantic Ocean from Sept $25^{th}-$ Oct 15^{th}. One of the tragedies of the storm was the sinking of the El Faro merchant vessel. As part of its investigations into the sinking of this ship NTSB has asked NCEP to develop a detailed estimate of wind and sea conditions for the periods surrounding this incident.

Using State-Of-the-Art wave and hurricane simulation models, NCEP has conducted high resolution simulations around the area of the accident for the period of concern. Results from these simulations have been validated with available records associated with this event from NHC and NDBC buoys. With a few exceptions the models do a very good job of reproducing the observations both in wind speeds and wave heights, leading to significant confidence in the results.

Simulations show that around the time of the accident the storm reached wind speeds up to and exceeding 100 knots. Corresponding wave heights varied from $7-10$ m, with peak periods in the $9-12$ s range. Spectral plots showed a complex wave field developing under the influence of strong turning winds with some locations showing signatures of crossing seas.

The spectral model used to simulate these conditions only provides estimates on the Significant wave height which is the average of the highest one - third waves. A separate study to determine the maximum waves using non linear statistical analysis in combination with the wave spectra from this study is on going and will be the subject of a companion report.

References

Alves, J. G. H. M., A. Chawla, H. L. Tolman, D. Schwab, G. Lang and G. Mann, 2014a: The operational implementation of a great lakes wave forecasting system at noaa/ncep. *Wea. & Forecast.*, **29**, 1473 – 1497.

Alves, J. G. H. M., S. Stripling, A. Chawla, H. L. Tolman and A. van der Westhuysen, 2014b: Operational wave guidance at the us national weather service during tropical/posttropical storm sandy, october 2012. *Mon. Wea. Rev.*, **143**, 1687 – 1702.

Chawla, A., D. Spindler and H. L. Tolman, 2013a: Validation of a thirty year wave hindcast using the climate forecast system reanalysis winds. *Ocean Modelling*, **70**, 189 – 206.

Chawla, A., H. L. Tolman, V. Gerald, D. Spindler, T. Spindler, J.-H. G. M. Alves, D. Cao, J. L. Hanson and E.-M. Devalier, 2013b: A multi grid wave forecasting model: A new paradigm in operational wave forecasting. *Wea. & Forecast.*, **28**, 1057 – 1078.

Derber, J. C., D. F. Parrish and S. J. Lord, 1991: The new global operational analysis system at the National Meteorological Center. *Wea. & Forecast.*, **6**, 538–547.

Kanamitsu, M., 1989: Description of the NMC global data assimilation and forecast system. *Wea. & Forecast.*, **4**, 335–342.

Tallapragada, V., L. Bernardet, M. K. Biswas, I. Ginis, Y. Kwon, Q. Liu, T. Marchok, D. Sheinin, B. Thomas, M. Tong, S. Trahan, W. Wang, R. Yablonsky and X. Zhang, 2015: Hurricane weather research and forecasting (HWRF) model: 2015 scientific documentation. Tech. rep., Development Test Bed Center, 113 pp [available online at http://www.dtcenter.org/HurrWRF/users/docs/scientific_documents/HWRF_v3.7a_SD.pdf].

Tolman, H. L., 2002: User manual and system documentation of WAVEWATCH III version 2.22. Tech. Note 222, NOAA/NWS/NCEP/MMAB, 133 pp.

Tolman, H. L., 2009: User manual and system documentation of WAVEWATCH III version 3.14. Tech. Note 276, NOAA/NWS/NCEP/MMAB, 220 pp.

Tolman, H. L., 2014: User manual and system documentation of WAVEWATCH III version 4.18. Tech. Note 316, NOAA/NWS/NCEP/MMAB, 311 pp.

Tolman, H. L., J. H. G. M. Alves and Y. Y. Chao, 2005: Operational forecasting of wind generated waves by hurricane isabel at ncep. *Wea. & Forecast.*, **20**, 544 – 557.

Tolman, H. L., B. Balasubramaniyan, L. D. Burroughs, D. V. Chalikov, Y. Y. Chao, H. S. Chen and V. M. Gerald, 2002: Development and implementation of wind generated ocean surface wave models at NCEP. *Wea. & Forecast.*, **17**, 311 – 333.

APPENDICES

This page is intentionally left blank.

A Spectral Plots for point output at select locations

The full 2D hourly spectra as function of frequency and direction have been output at select locations as identified in Table 2. Here we provide the spectra polar plots for locations of interest (identified by the ElFaro* identifier in the table). Radial direction corresponds to frequency with lower frequencies closer to the center. Angular direction corresponds to the direction in which the waves are going, with the top of the circle corresponding to true North and the bottom to true South. The energy scales from Blue (low) to Red (high). Wind direction is given by the arrow in the center of each polar plot with the size of the arrow being scaled to the wind speed. The total Significant wave height, which is a measure of the overall wave energy in the spectrum is also given for each plot.

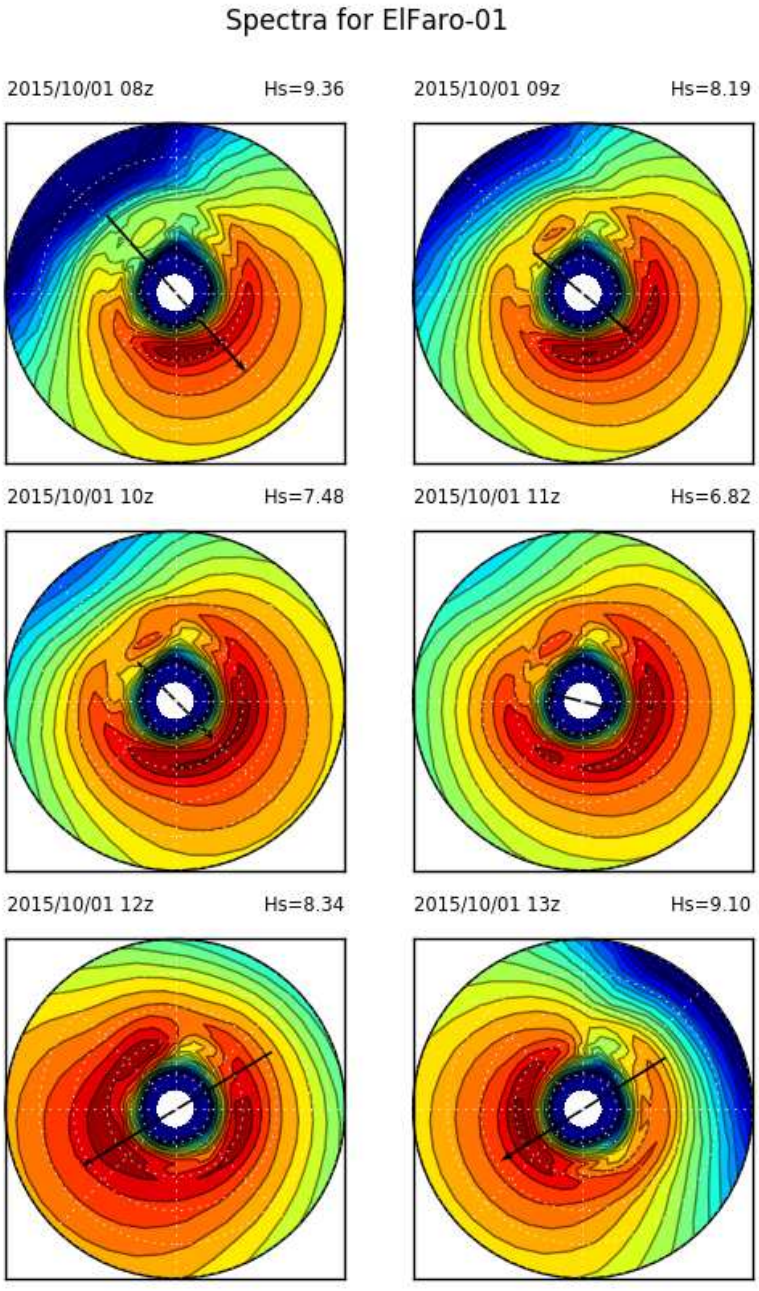

Figure 27: Spectral plot for point ElFaro-01

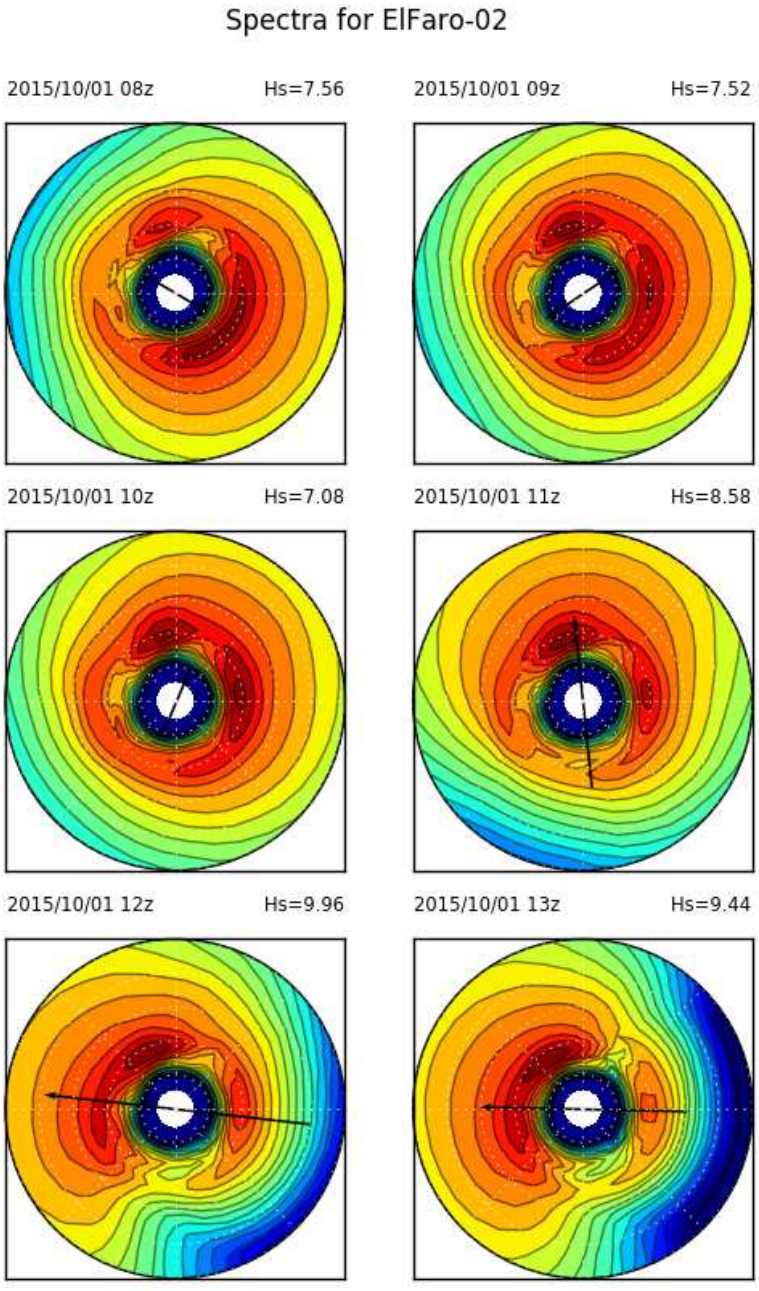

Figure 28: Spectral plot for point ElFaro-02

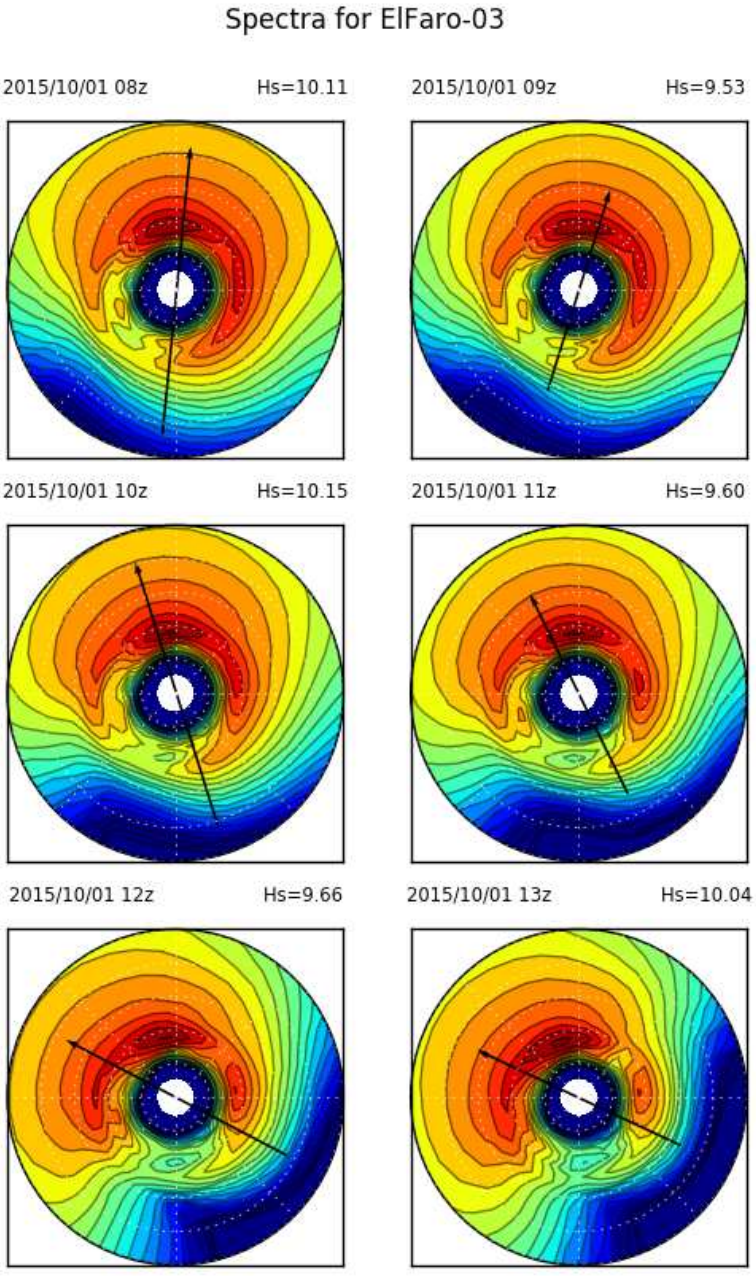

Figure 29: Spectral plot for point ElFaro-03

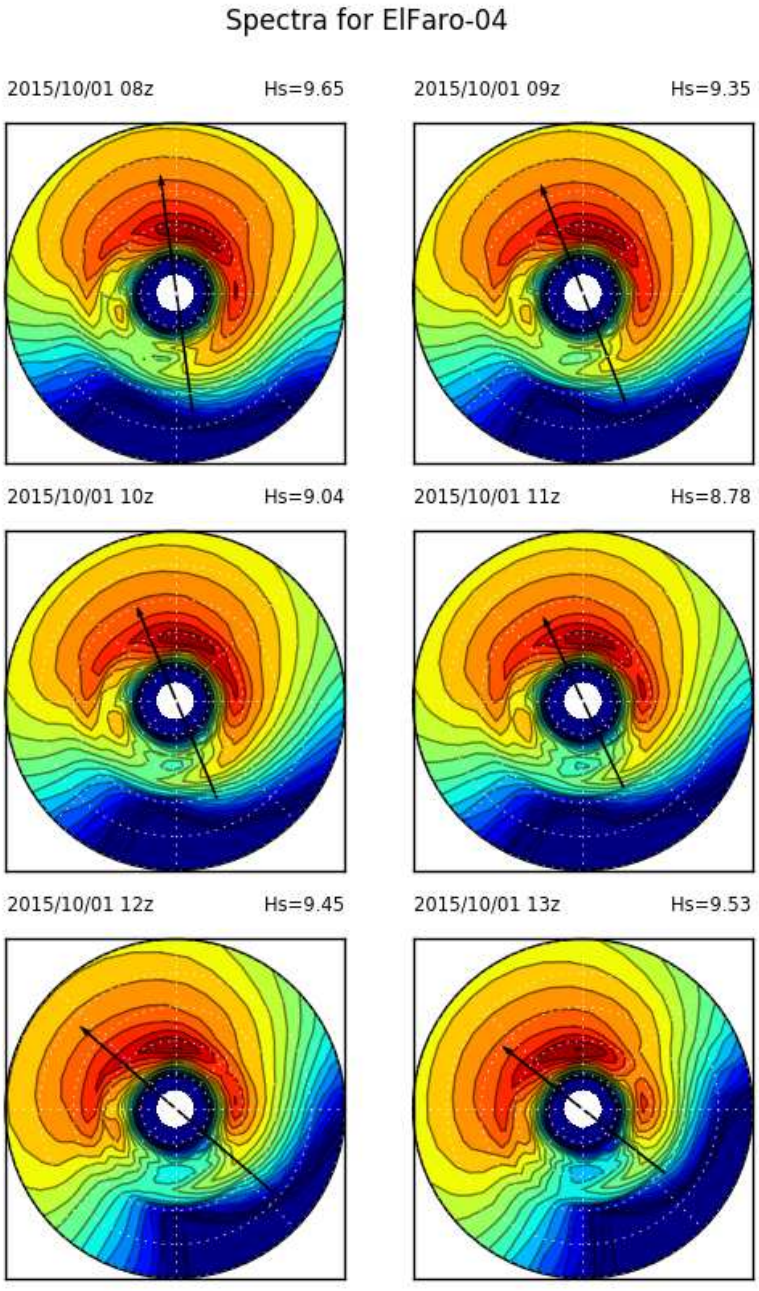

Figure 30: Spectral plot for point ElFaro-04

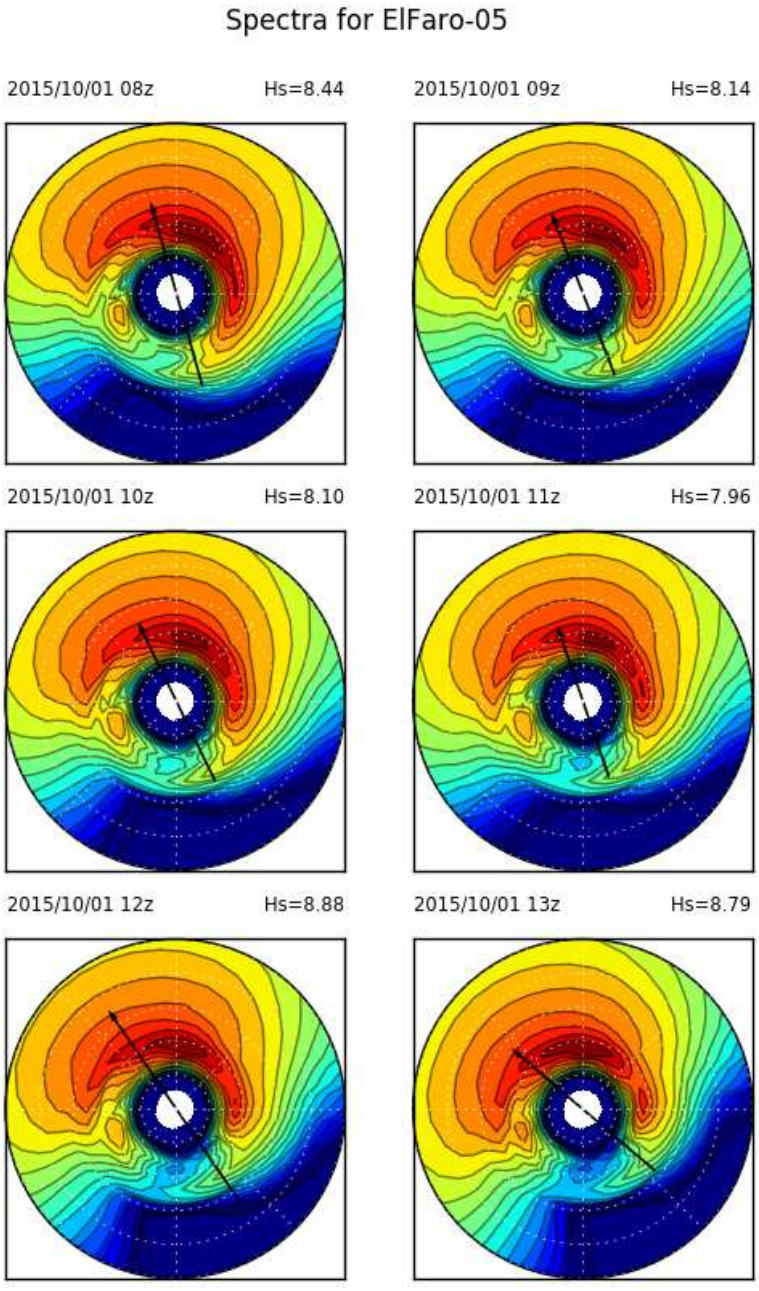

Figure 31: Spectral plot for point ElFaro-05

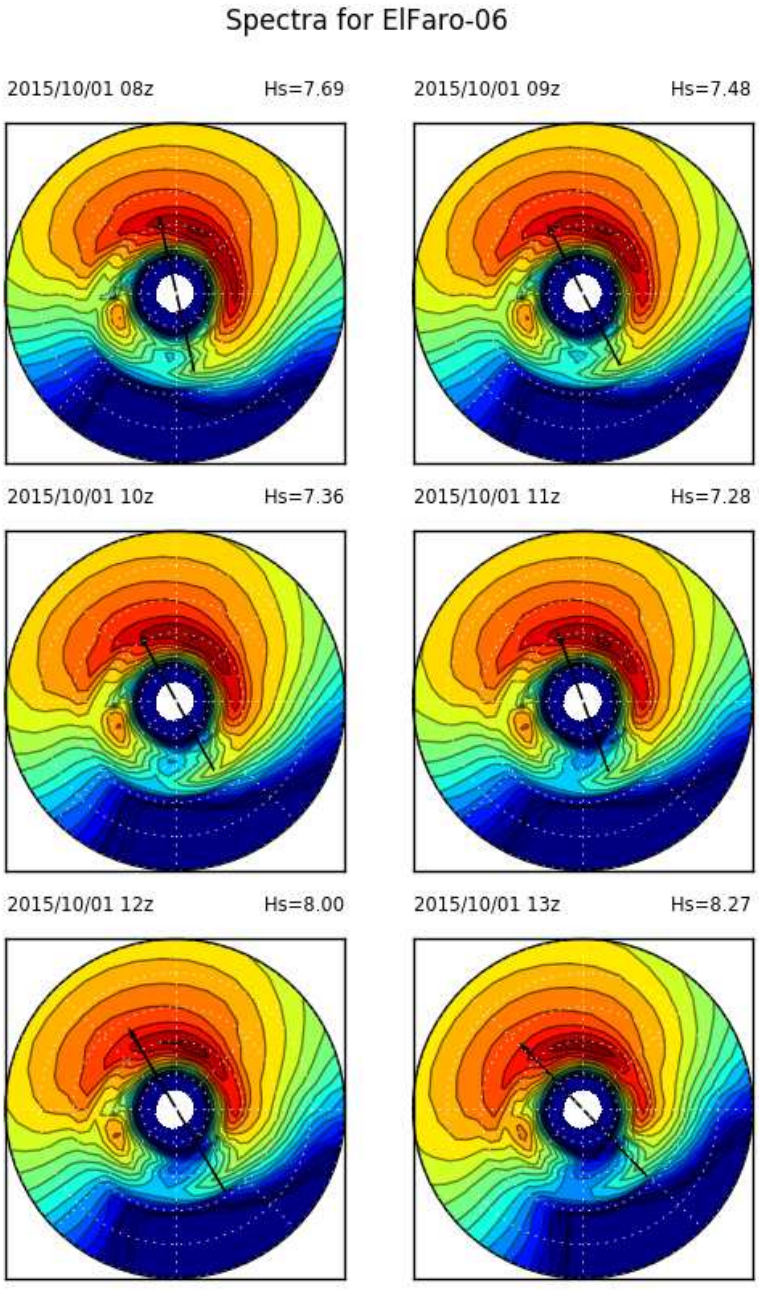

Figure 32: Spectral plot for point ElFaro-06

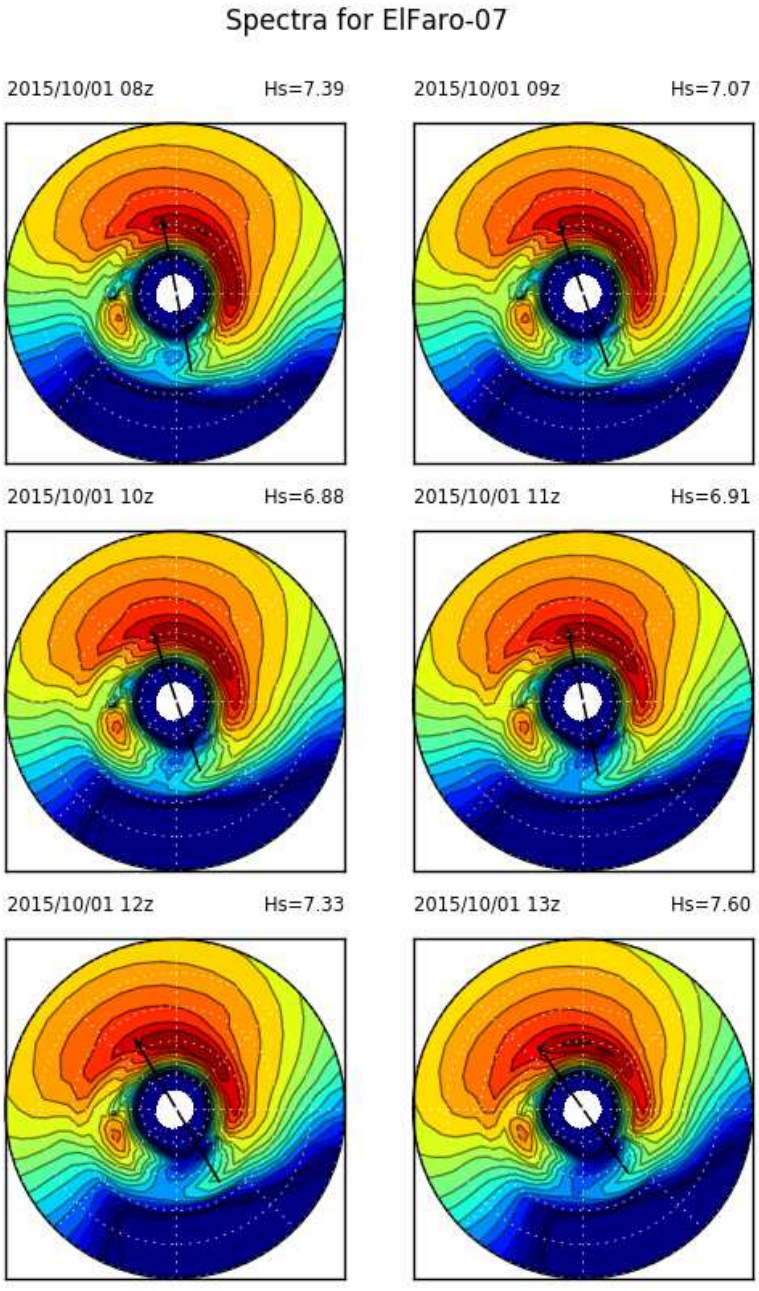

Figure 33: Spectral plot for point ElFaro-07

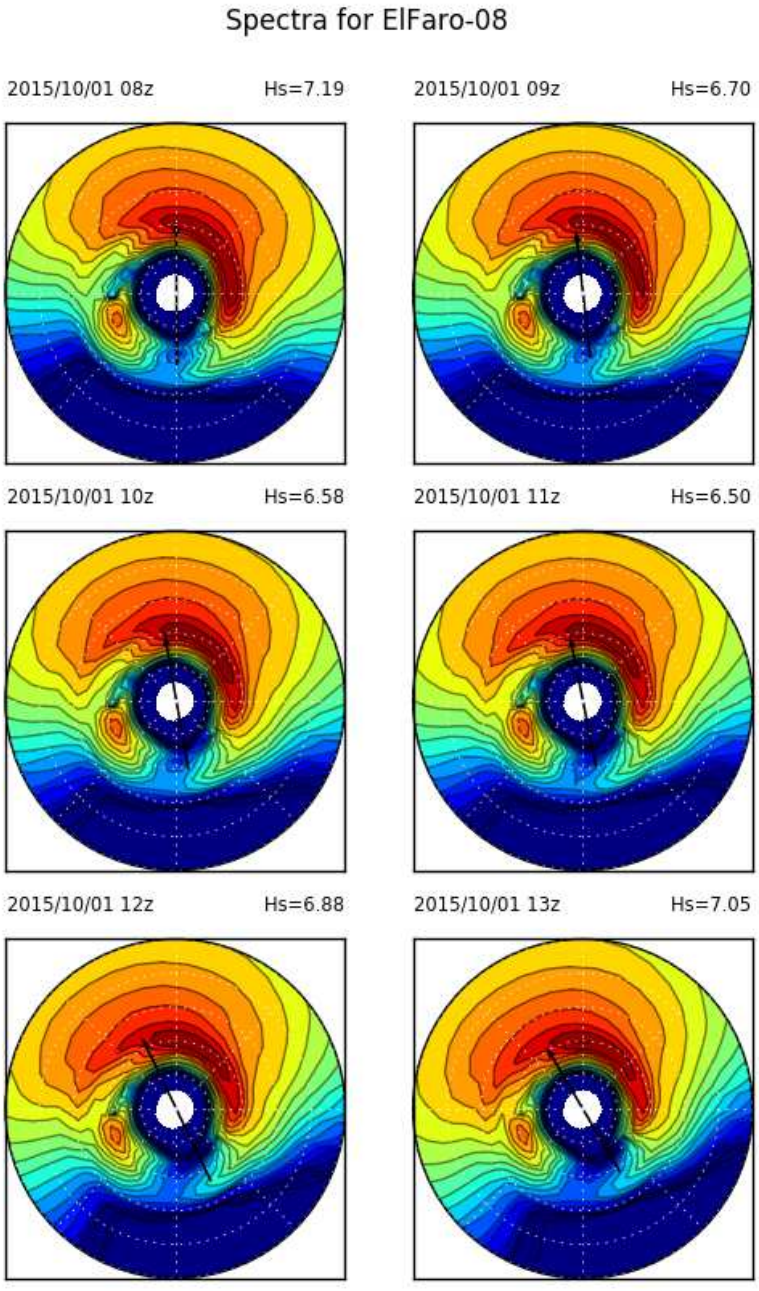

Figure 34: Spectral plot for point ElFaro-08

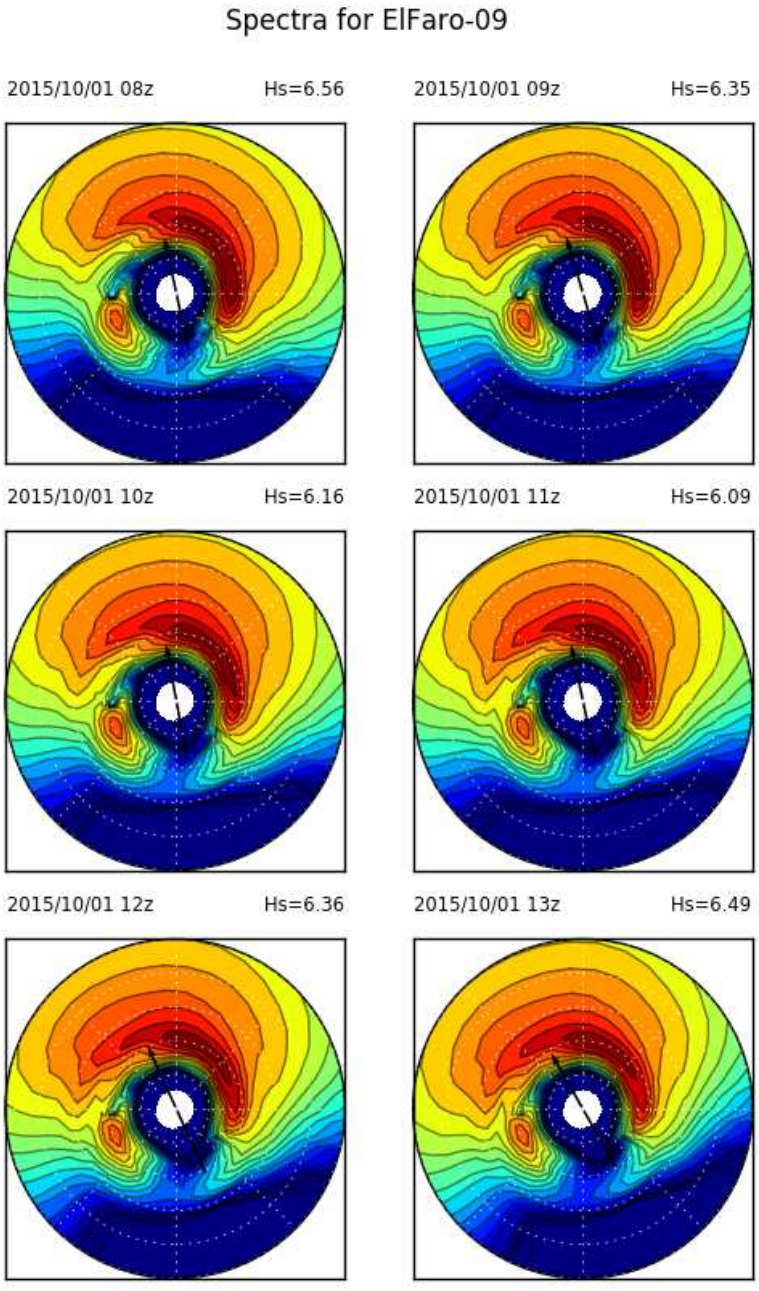

Figure 35: Spectral plot for point ElFaro-09

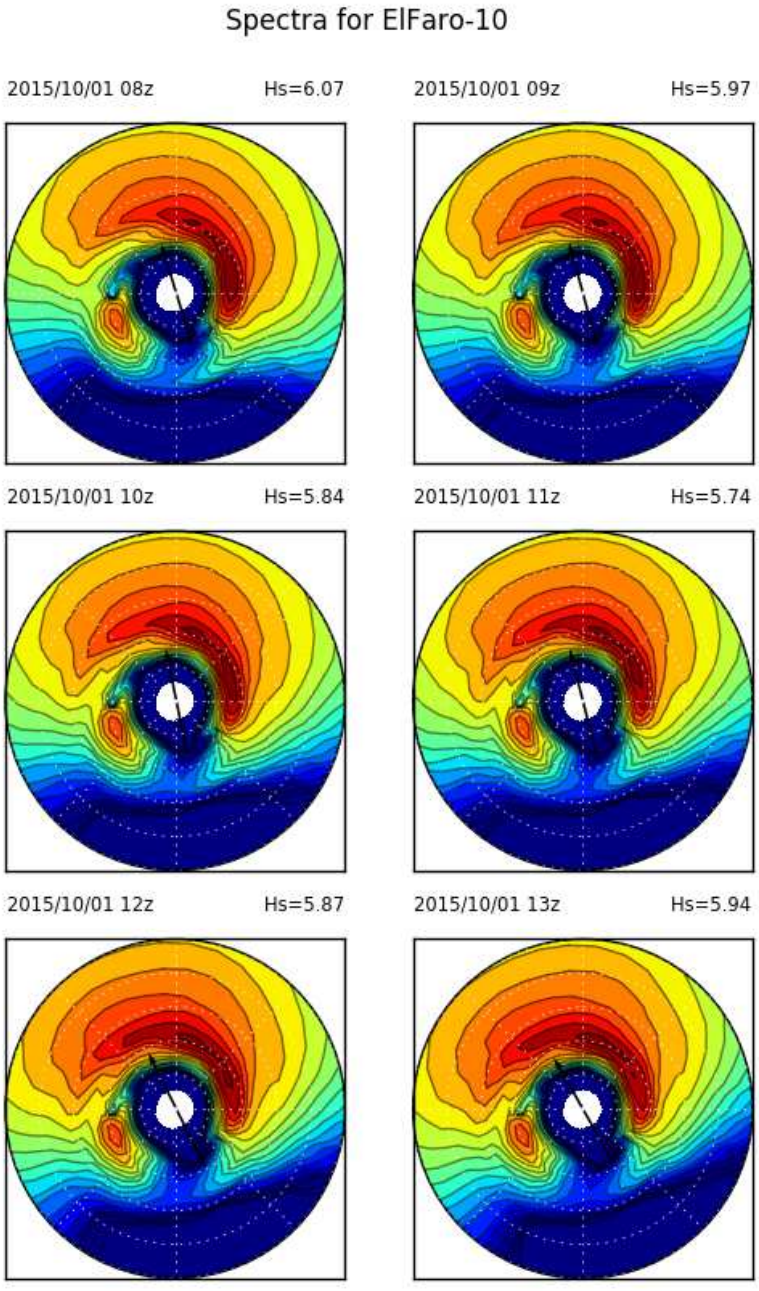

Figure 36: Spectral plot for point ElFaro-10

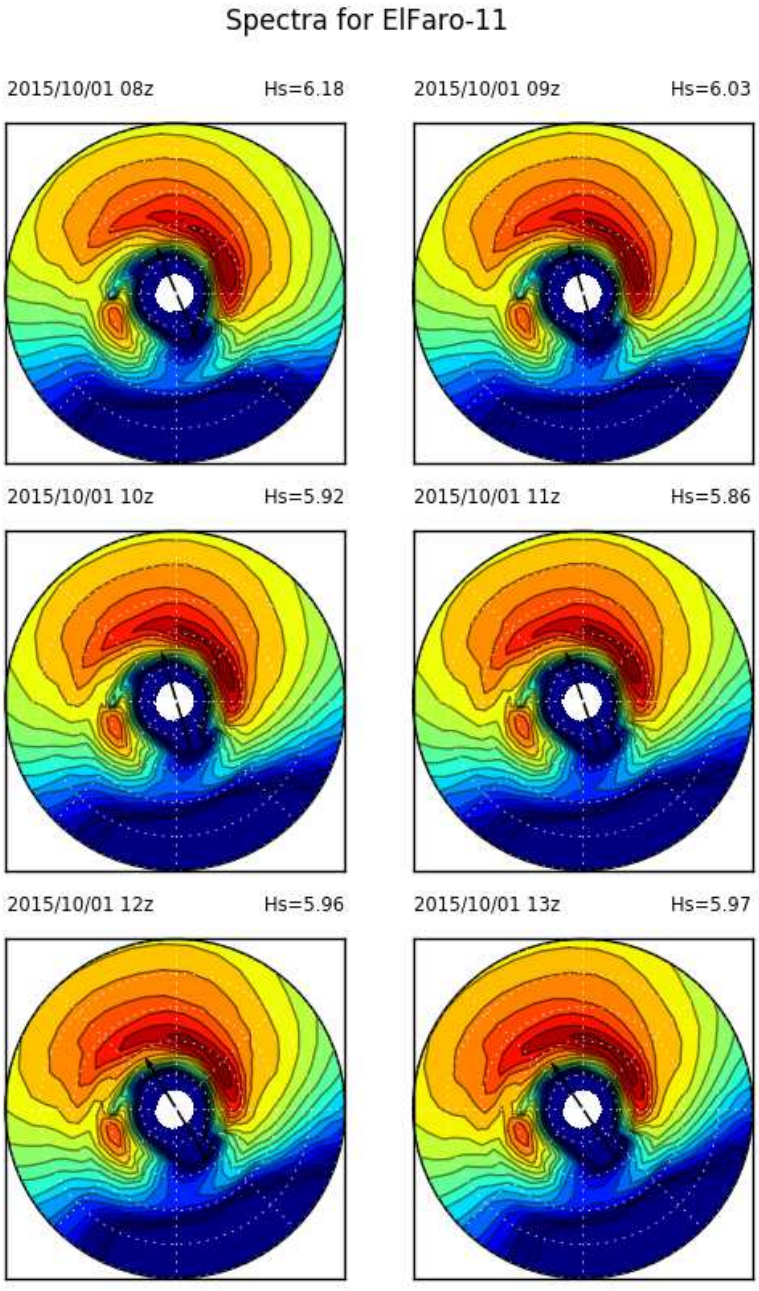

Figure 37: Spectral plot for point ElFaro-11

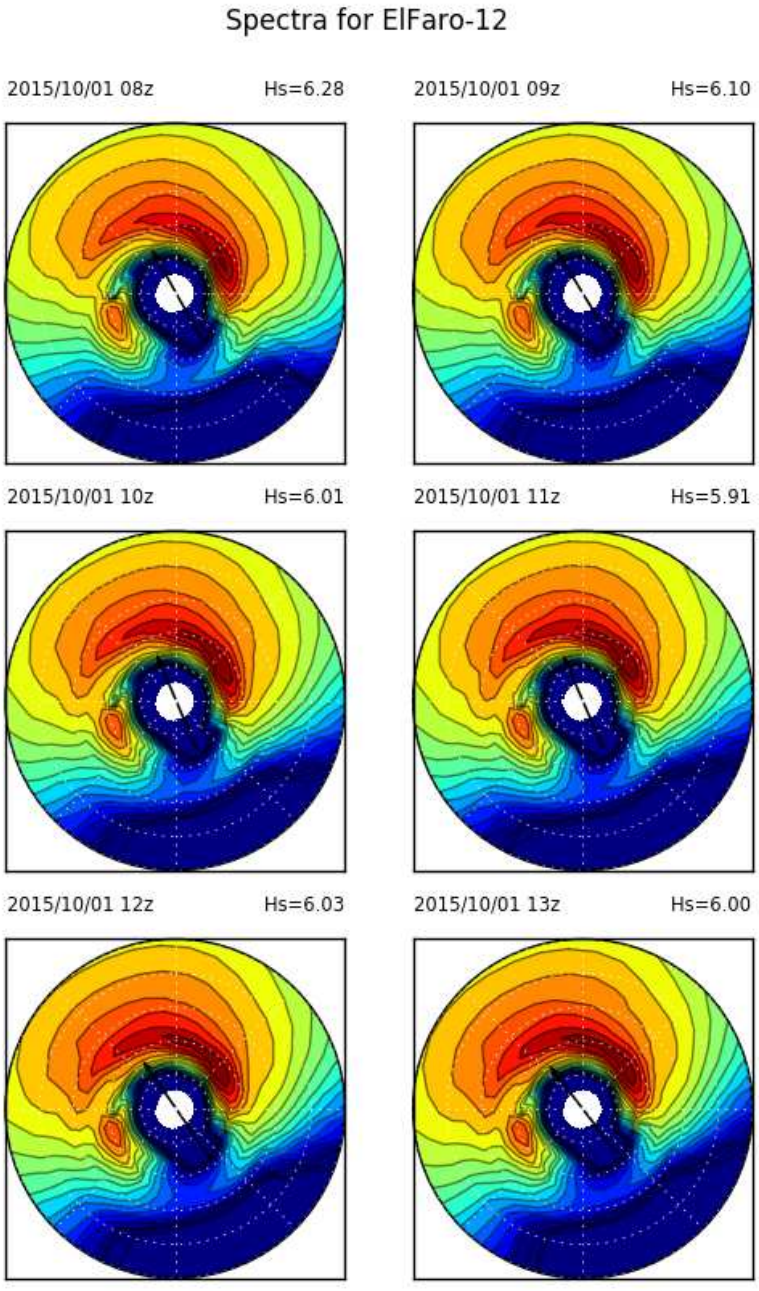

Figure 38: Spectral plot for point ElFaro-12

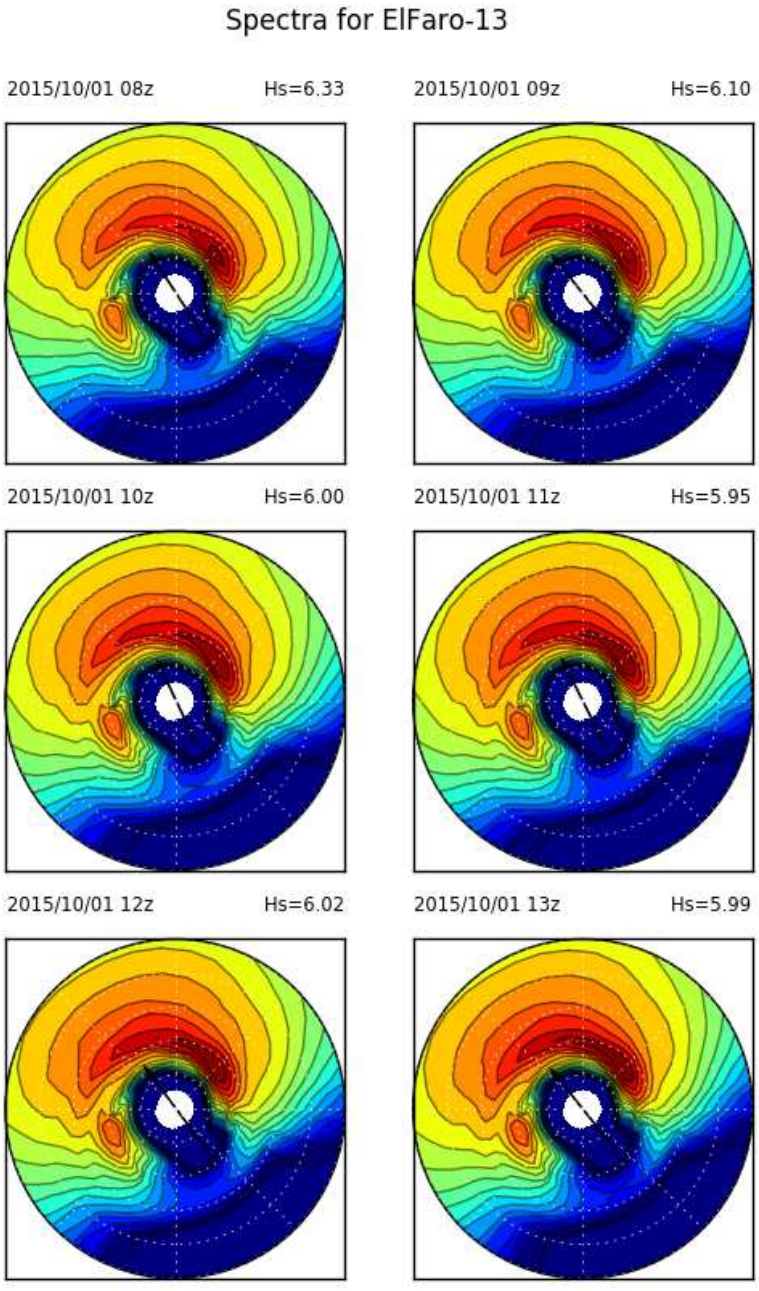

Figure 39: Spectral plot for point ElFaro-13

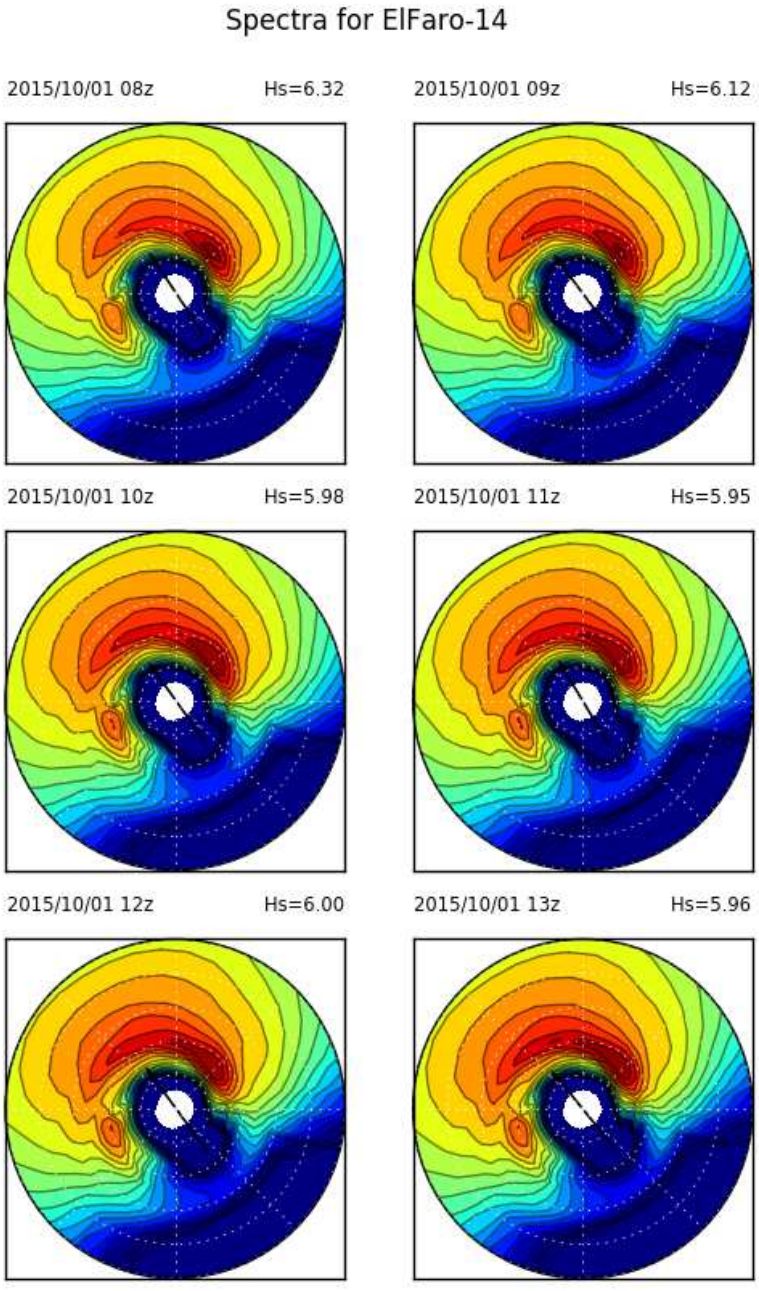

Figure 40: Spectral plot for point ElFaro-14

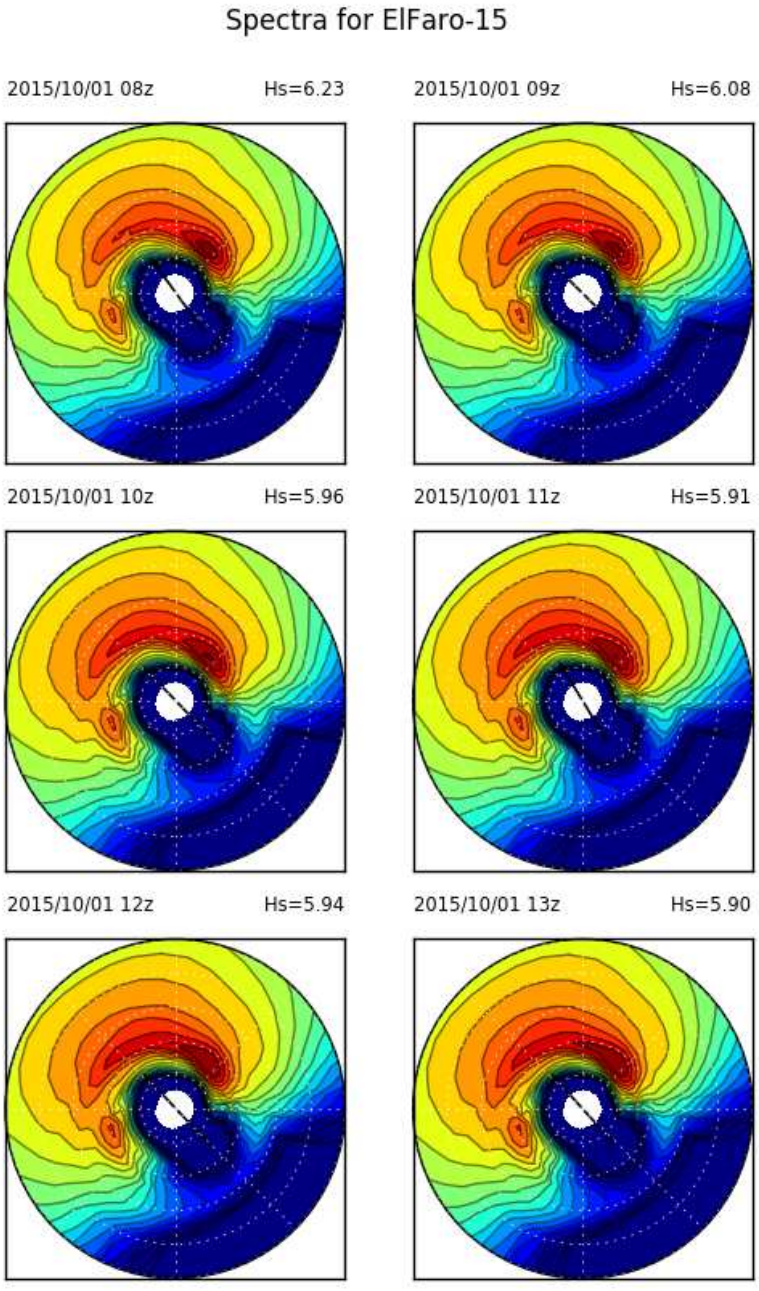

Figure 41: Spectral plot for point ElFaro-15

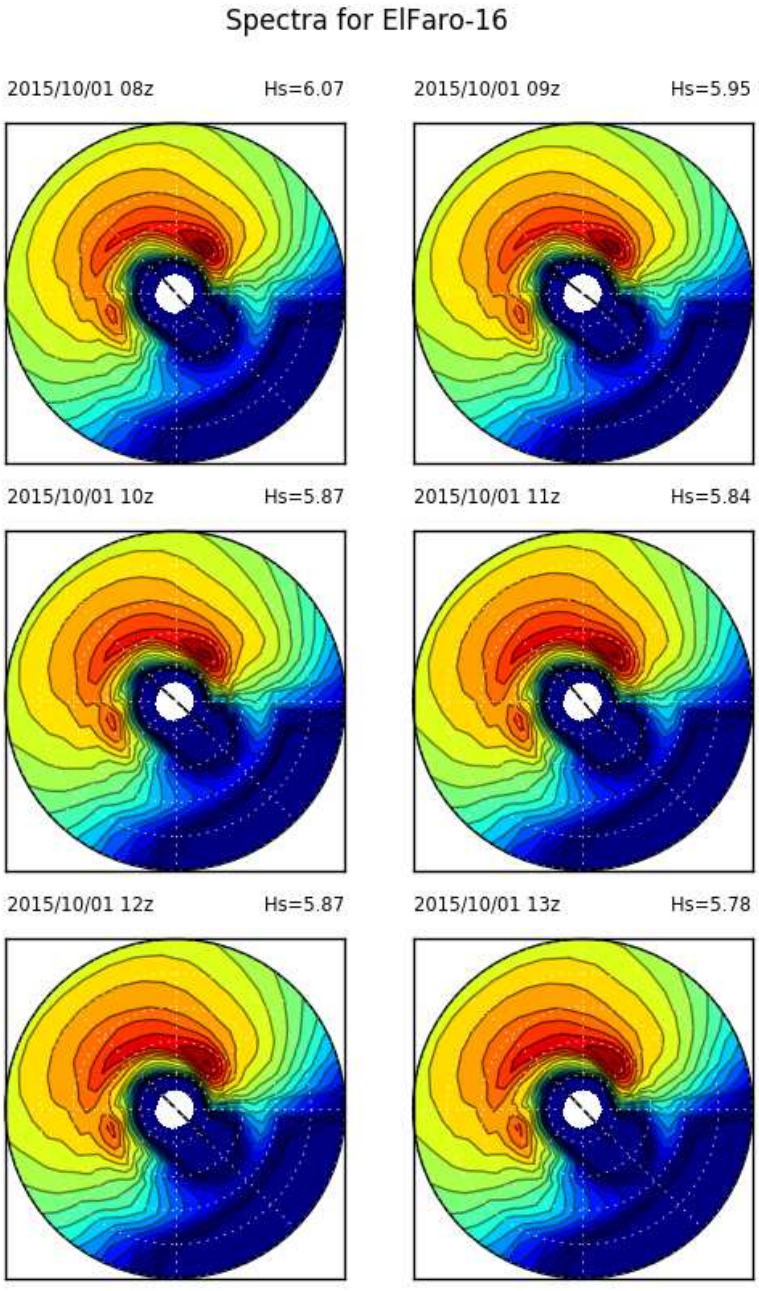

Figure 42: Spectral plot for point ElFaro-16

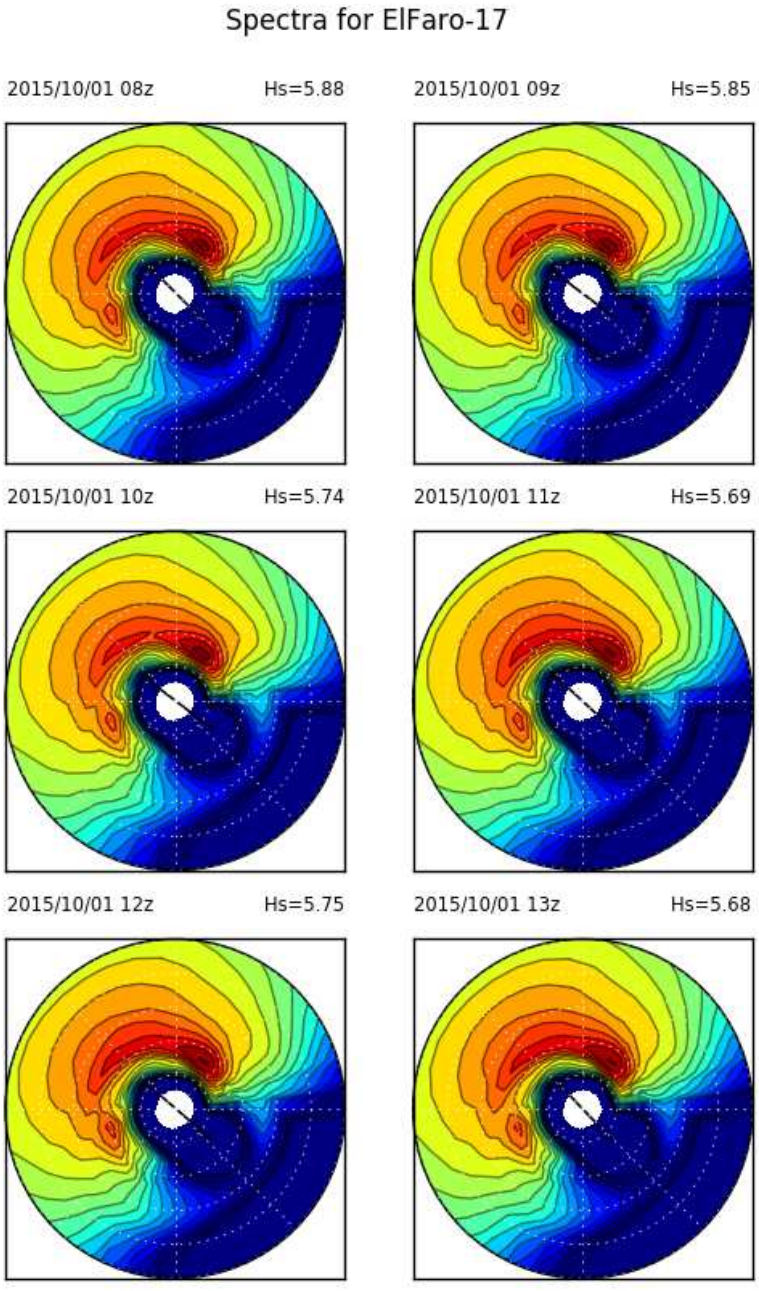

Figure 43: Spectral plot for point ElFaro-17

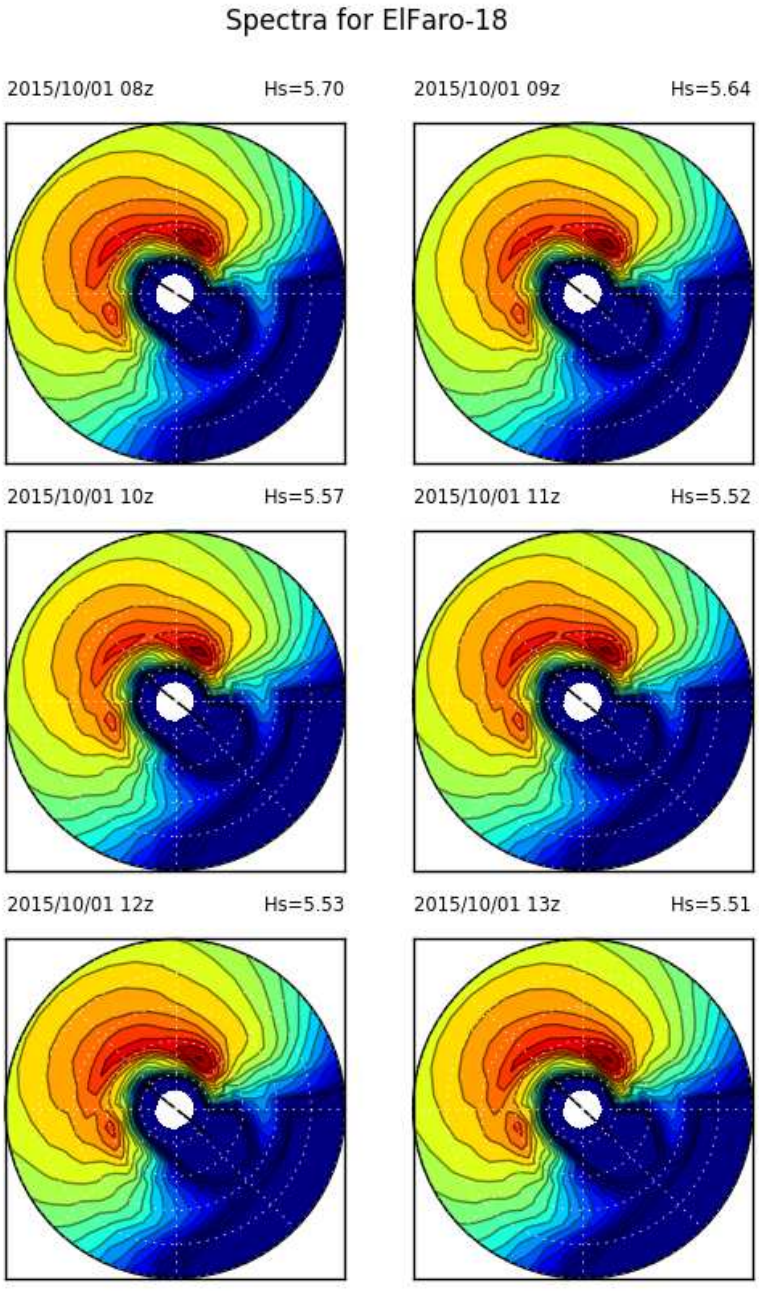

Figure 44: Spectral plot for point ElFaro-18

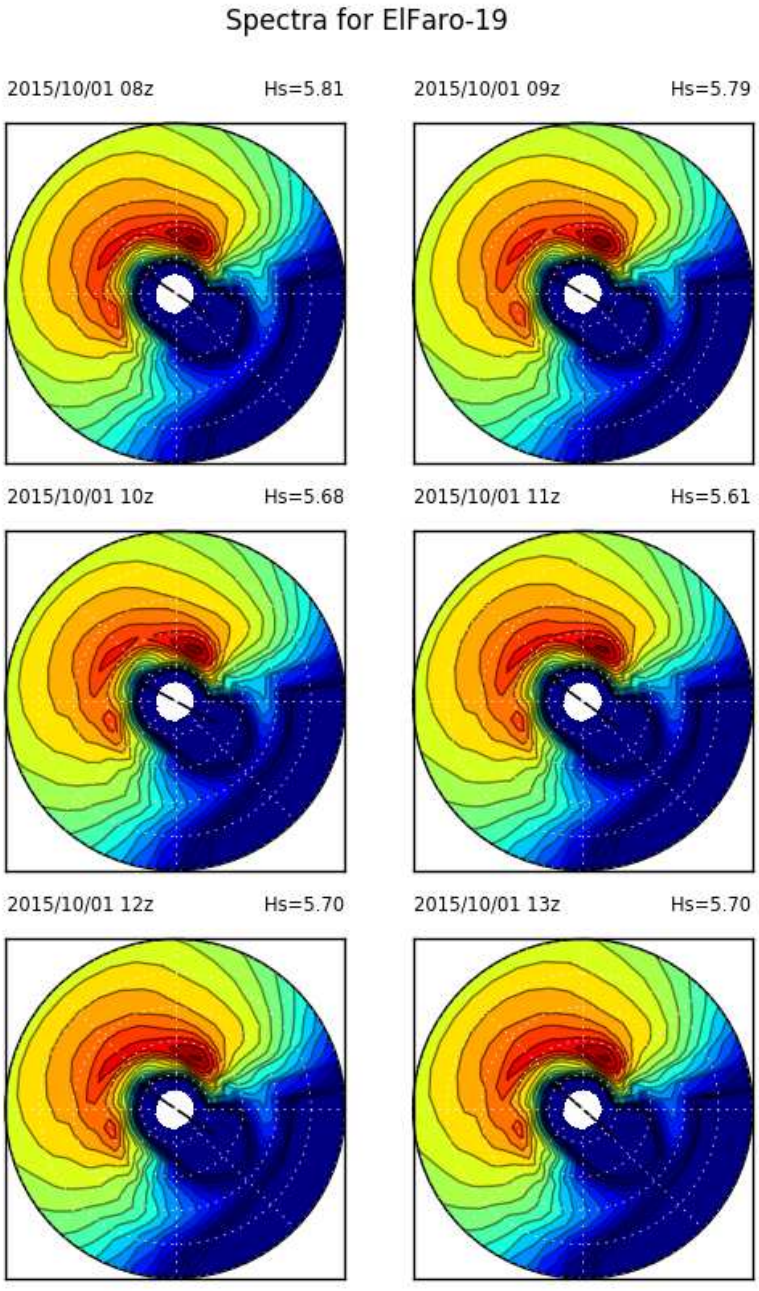

Figure 45: Spectral plot for point ElFaro-19

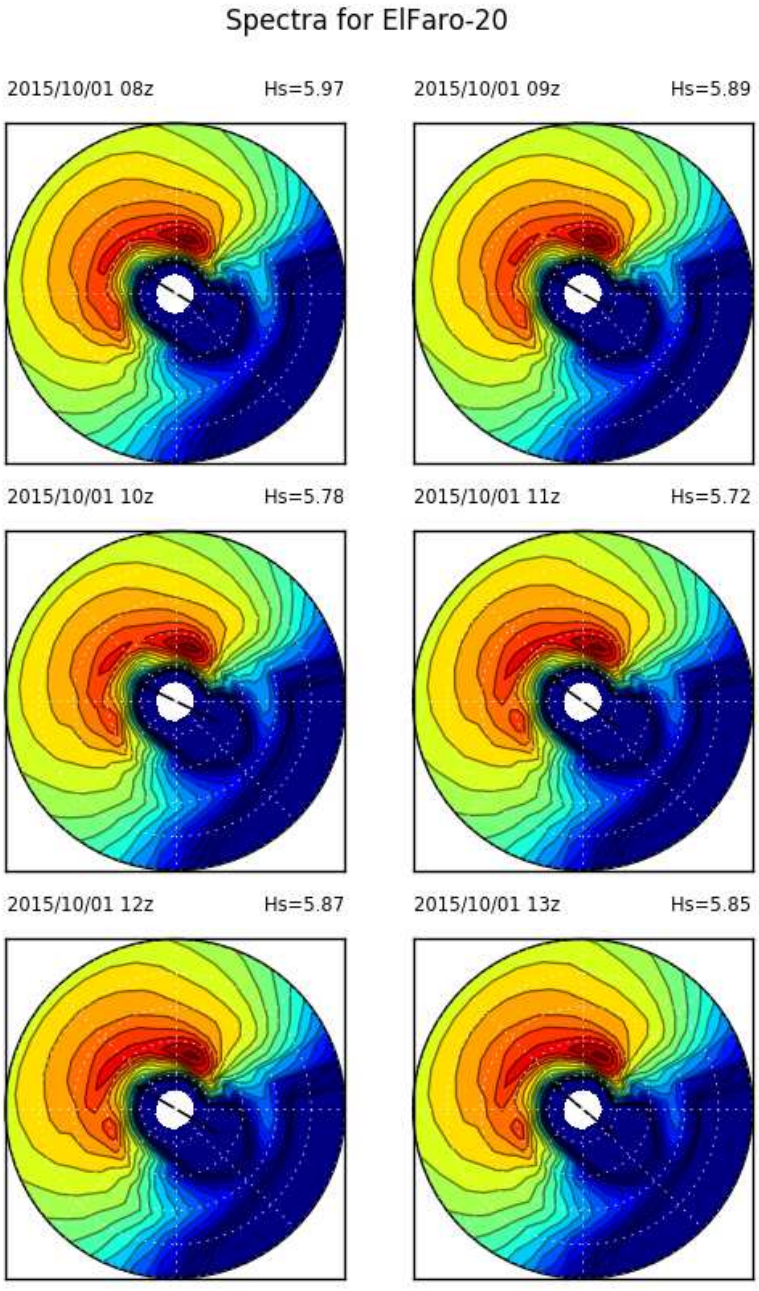

Figure 46: Spectral plot for point ElFaro-20

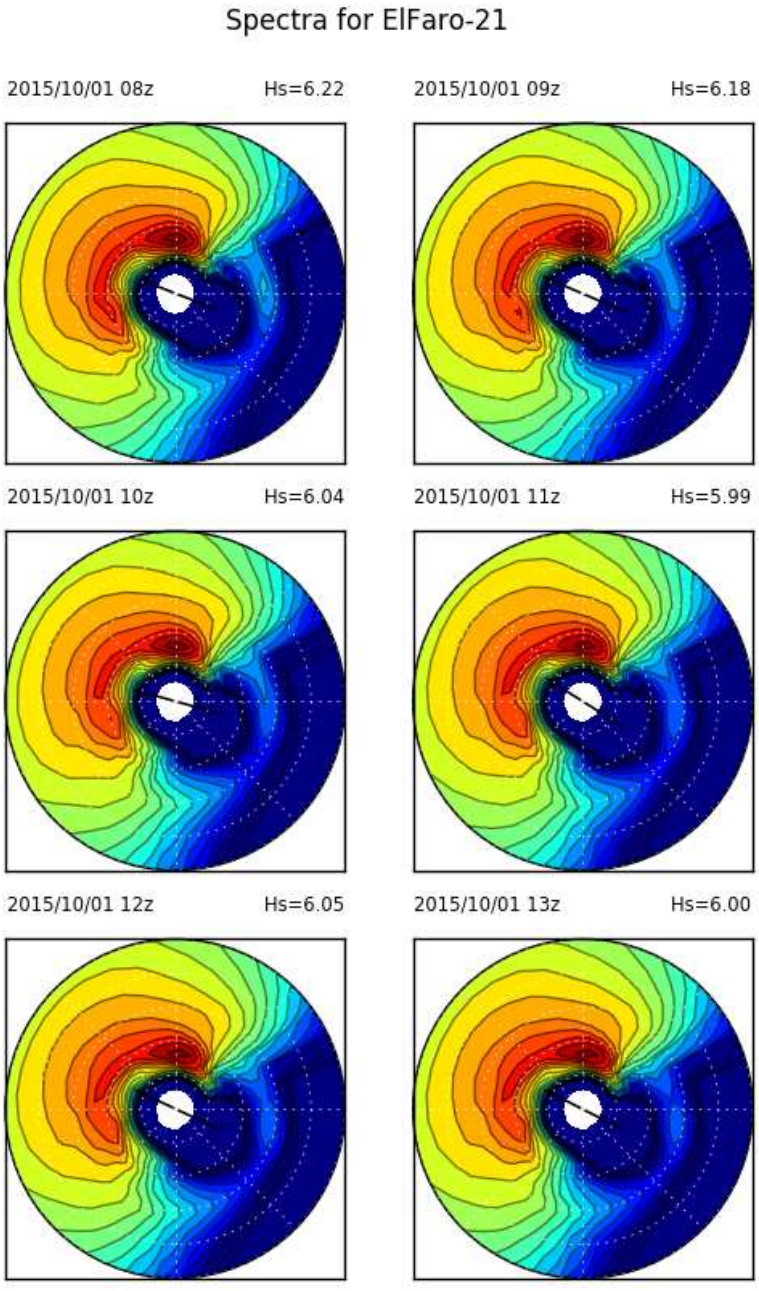

Figure 47: Spectral plot for point ElFaro-21

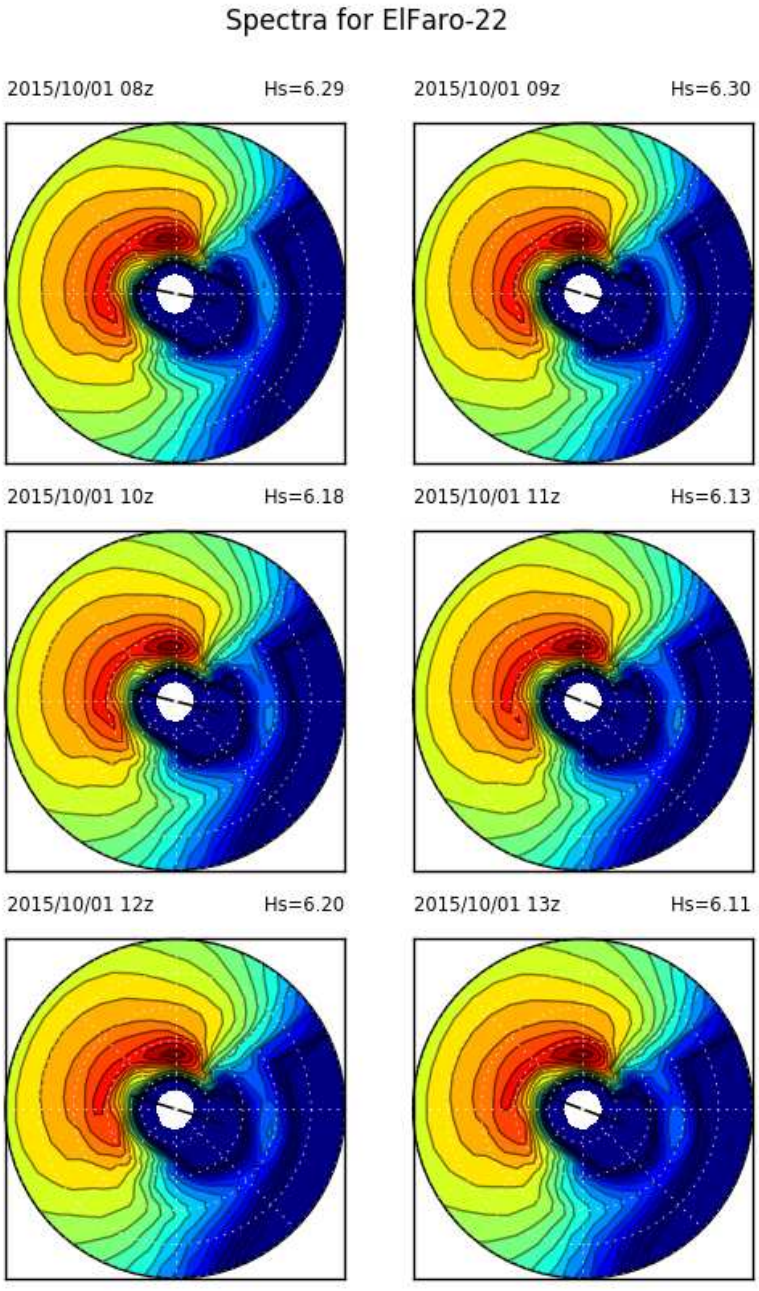

Figure 48: Spectral plot for point ElFaro-22

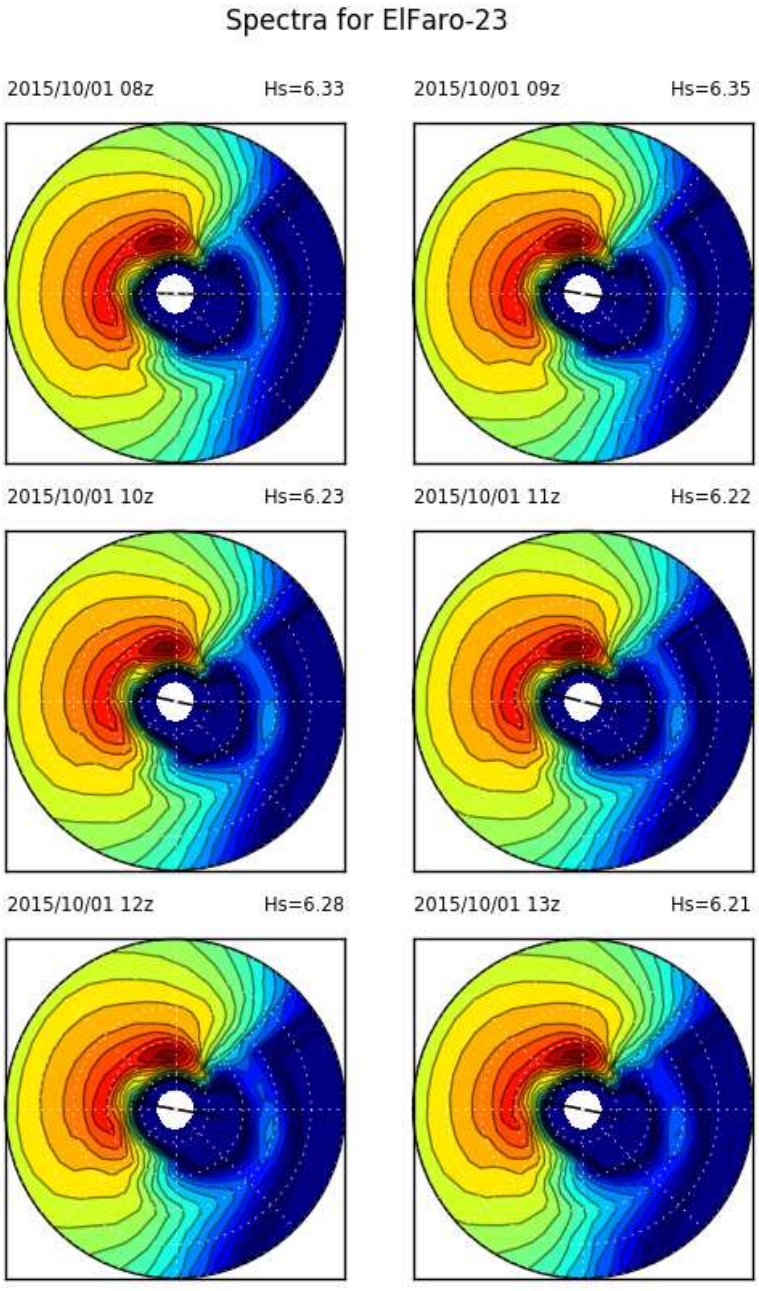

Figure 49: Spectral plot for point ElFaro-23

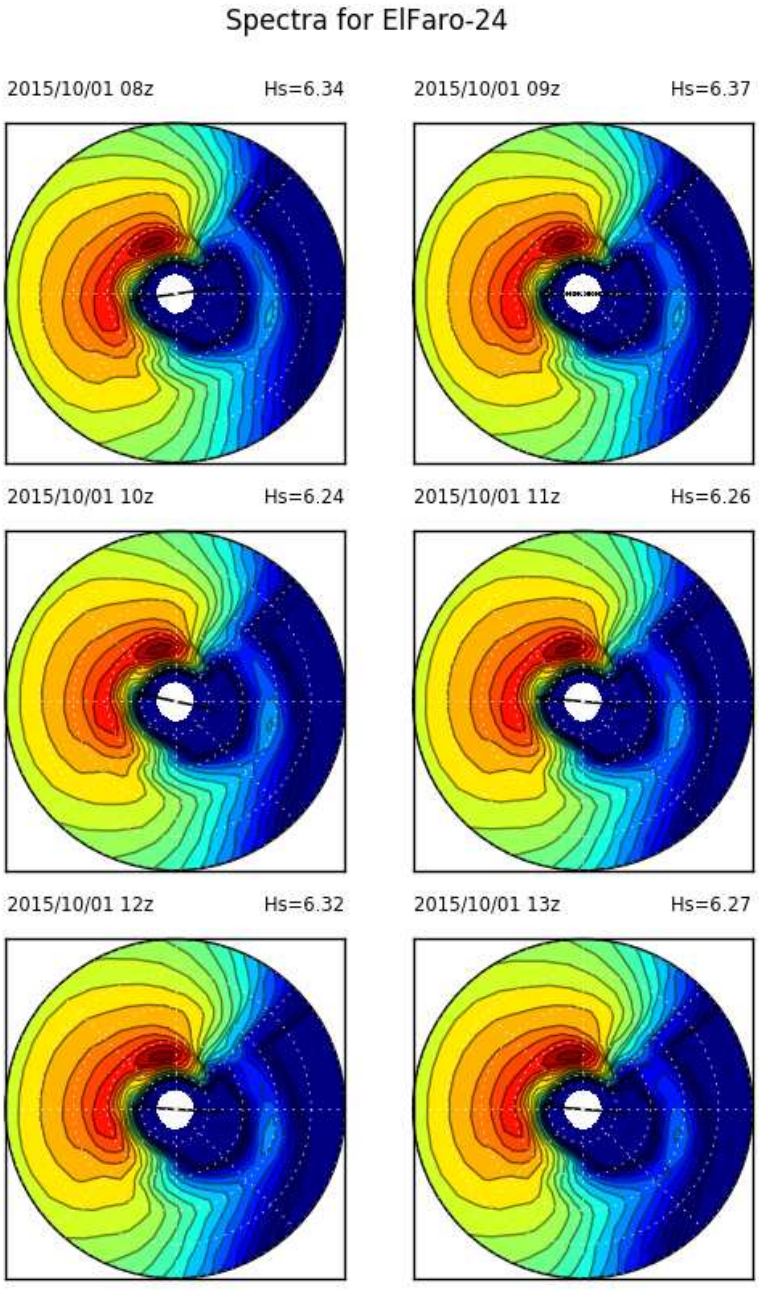

Figure 50: Spectral plot for point ElFaro-24

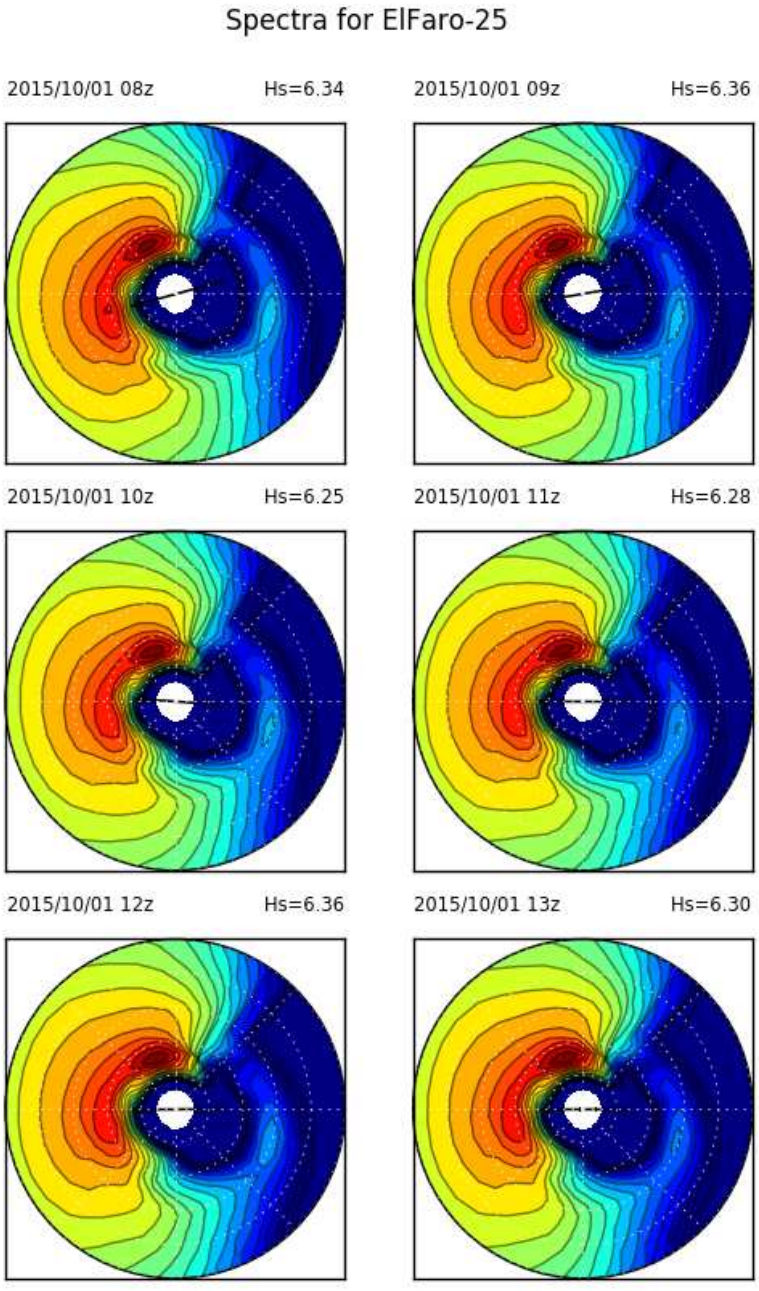

Figure 51: Spectral plot for point ElFaro-25

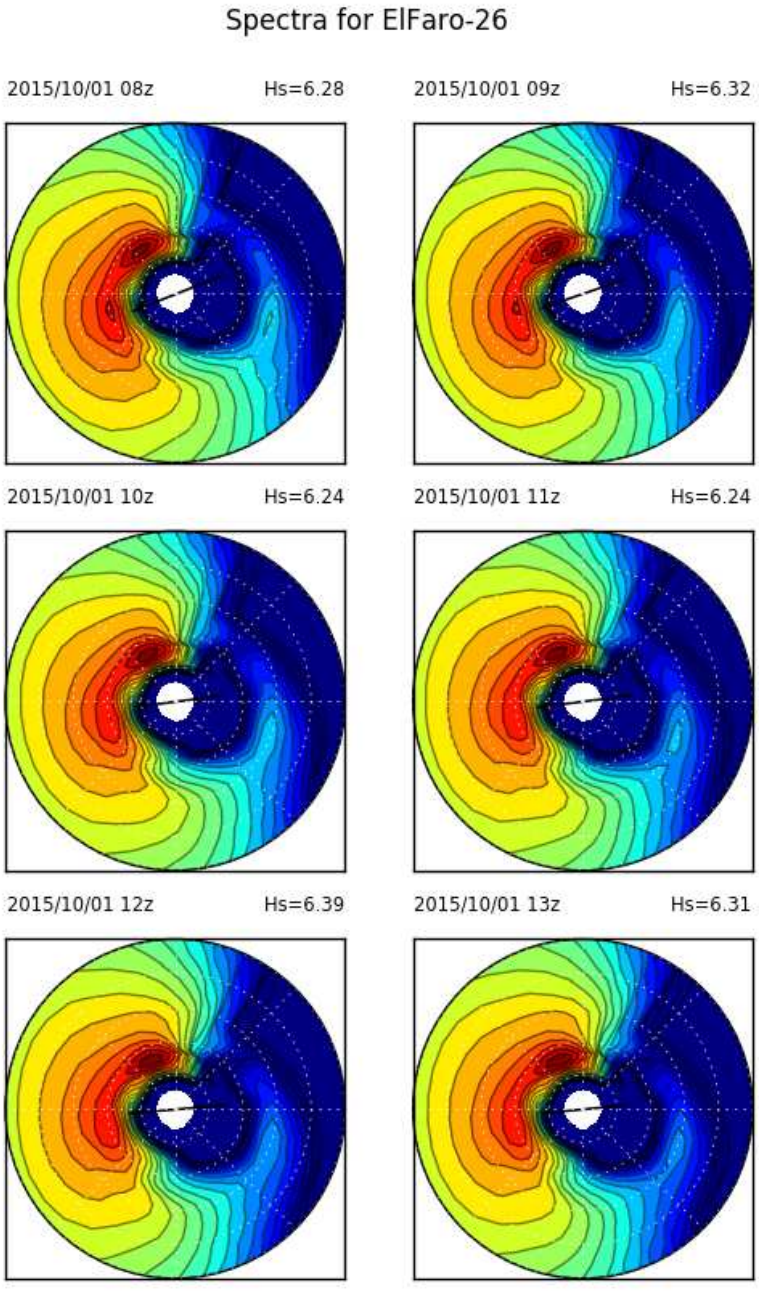

Figure 52: Spectral plot for point ElFaro-26

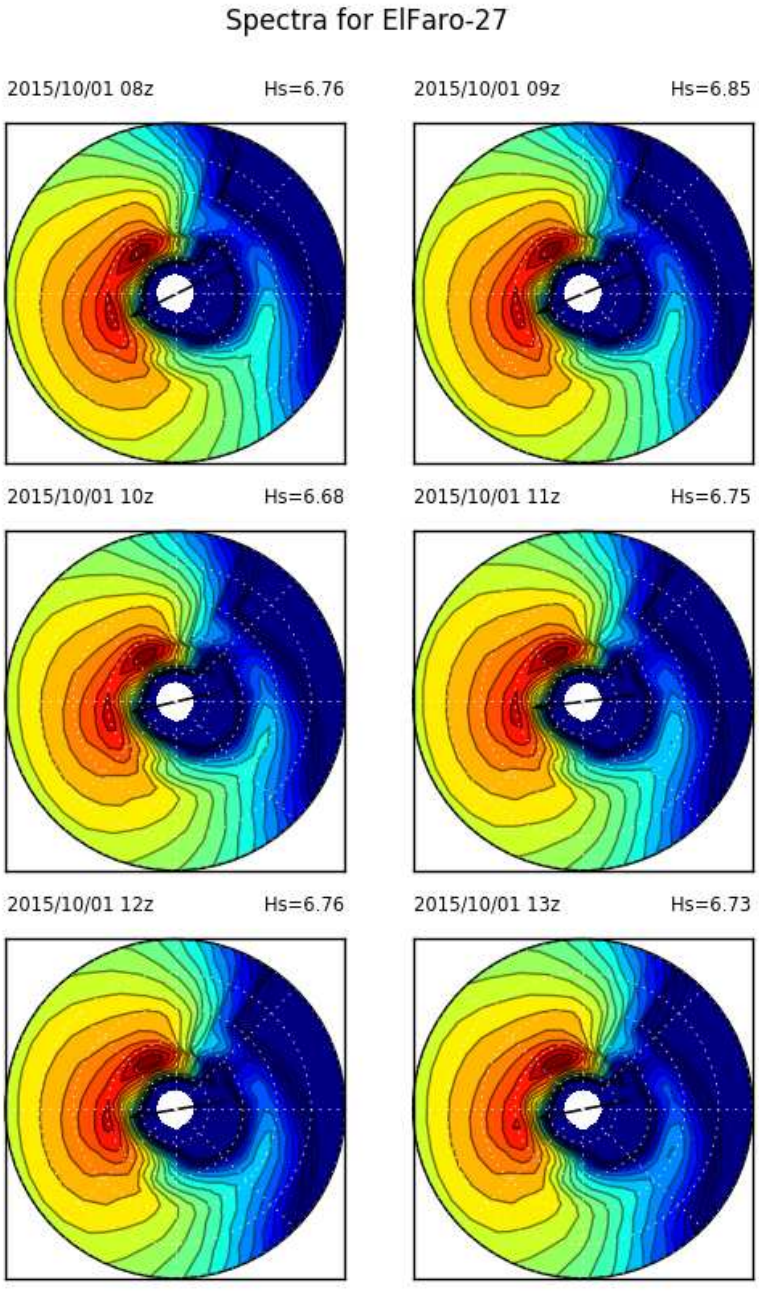

Figure 53: Spectral plot for point ElFaro-27

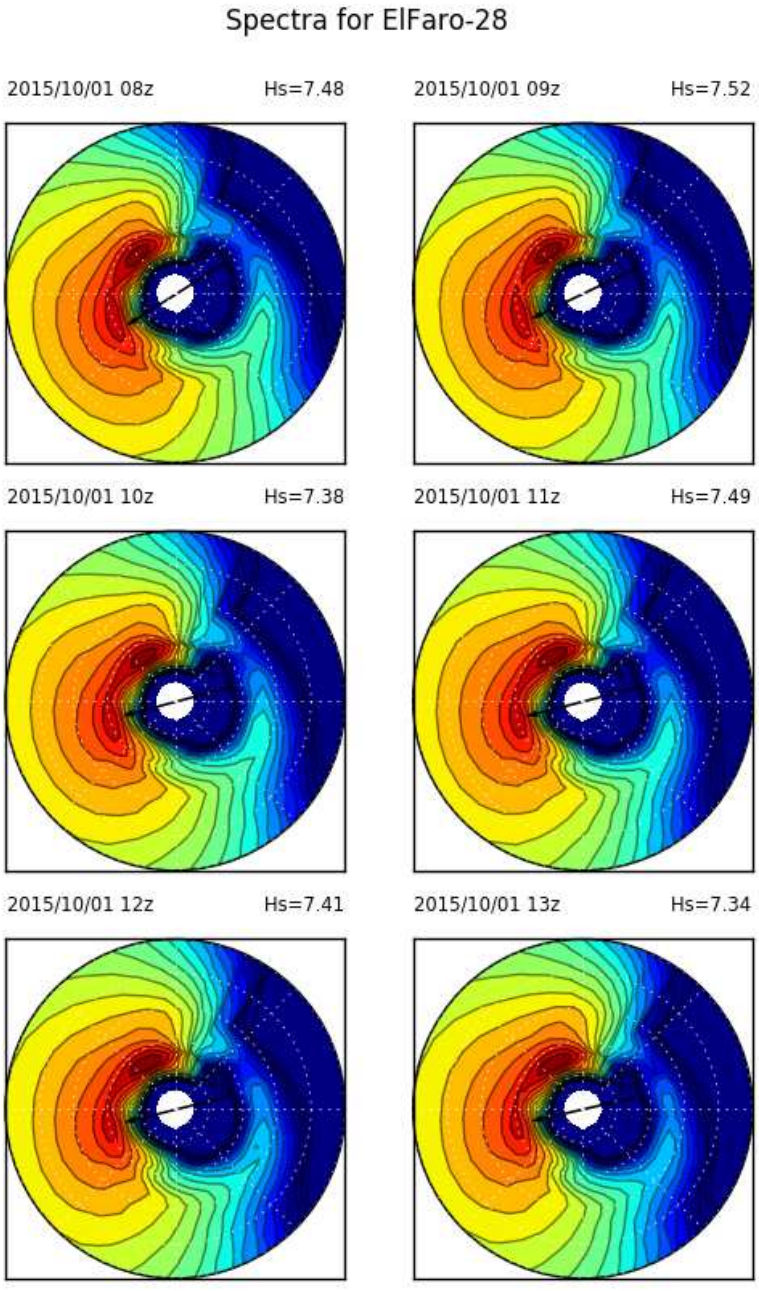

Figure 54: Spectral plot for point ElFaro-28

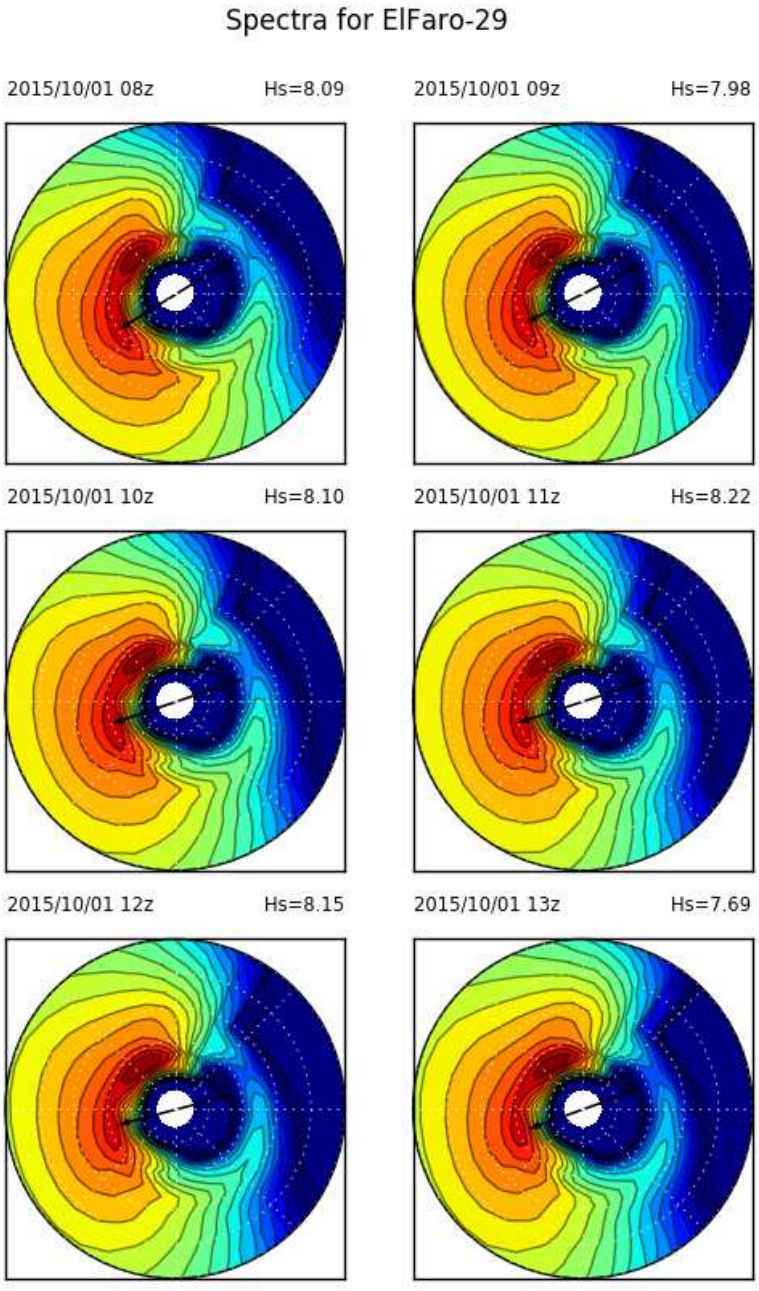

Figure 55: Spectral plot for point ElFaro-29

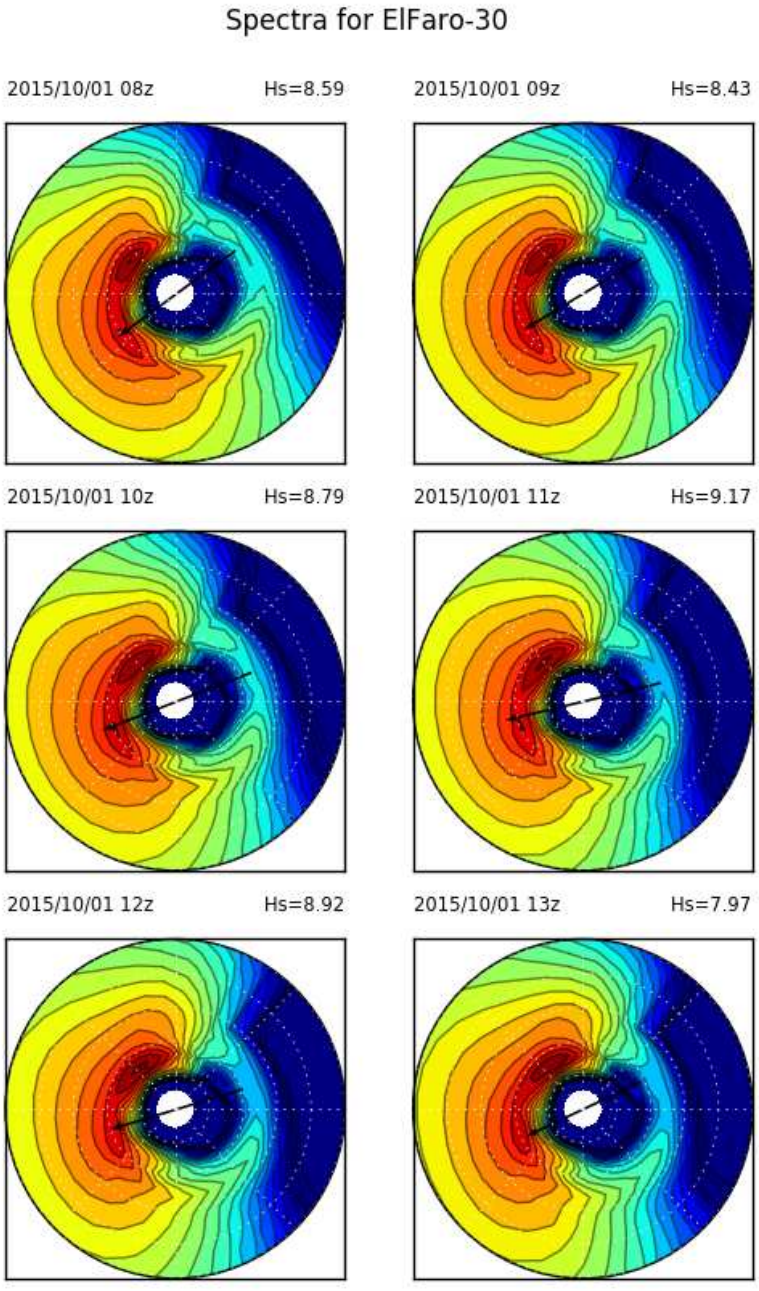

Figure 56: Spectral plot for point ElFaro-30

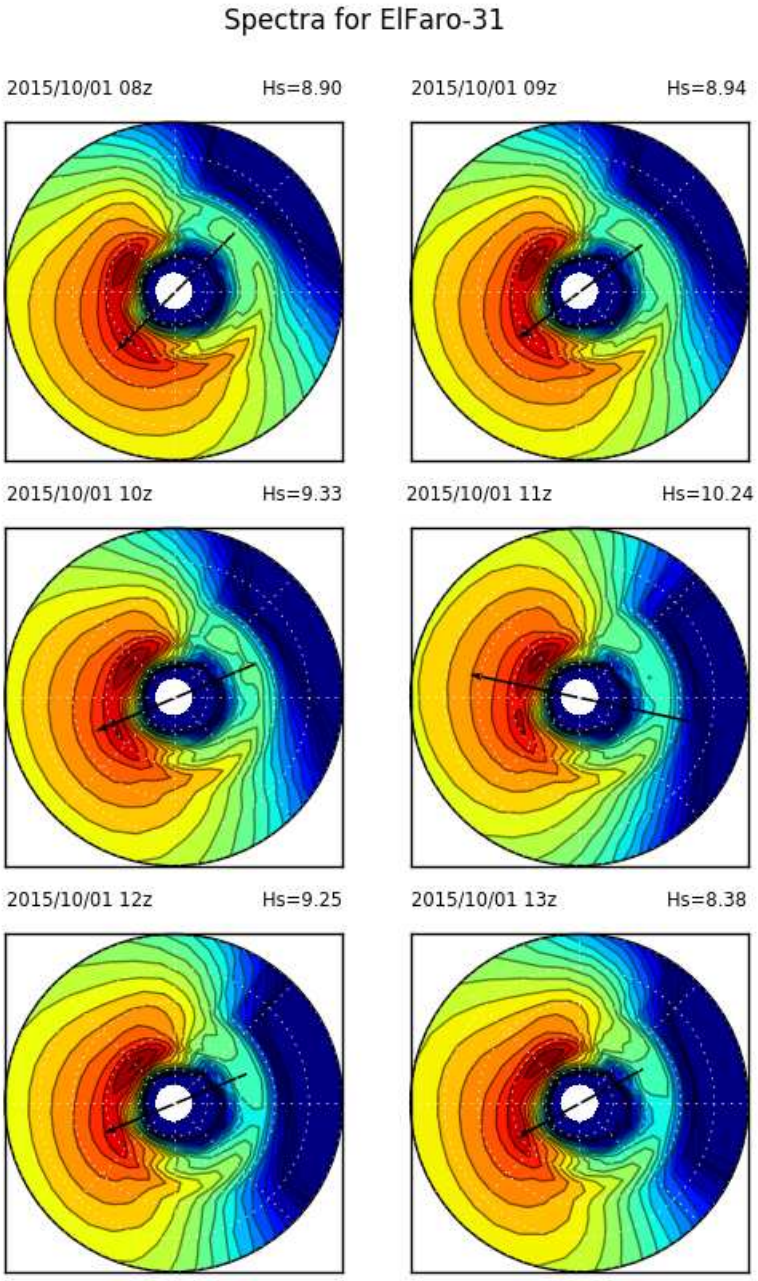

Figure 57: Spectral plot for point ElFaro-31

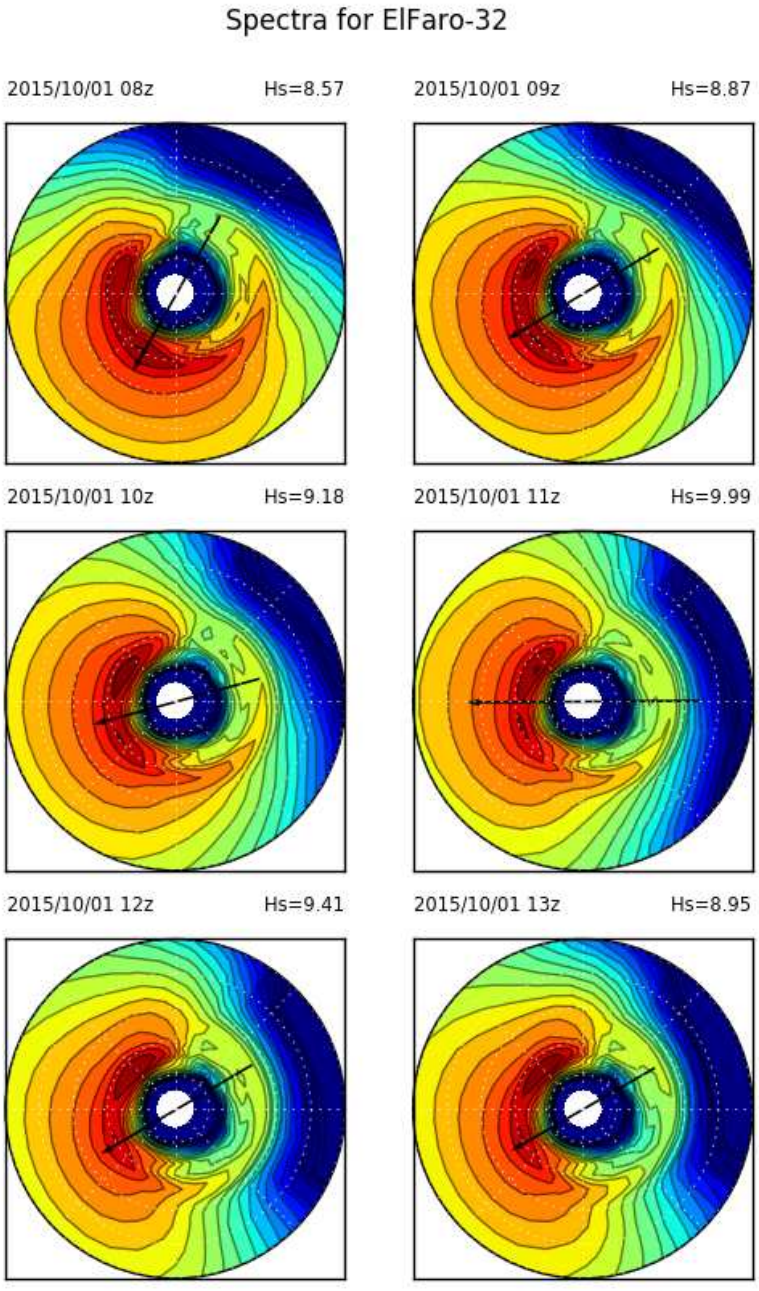

Figure 58: Spectral plot for point ElFaro-32

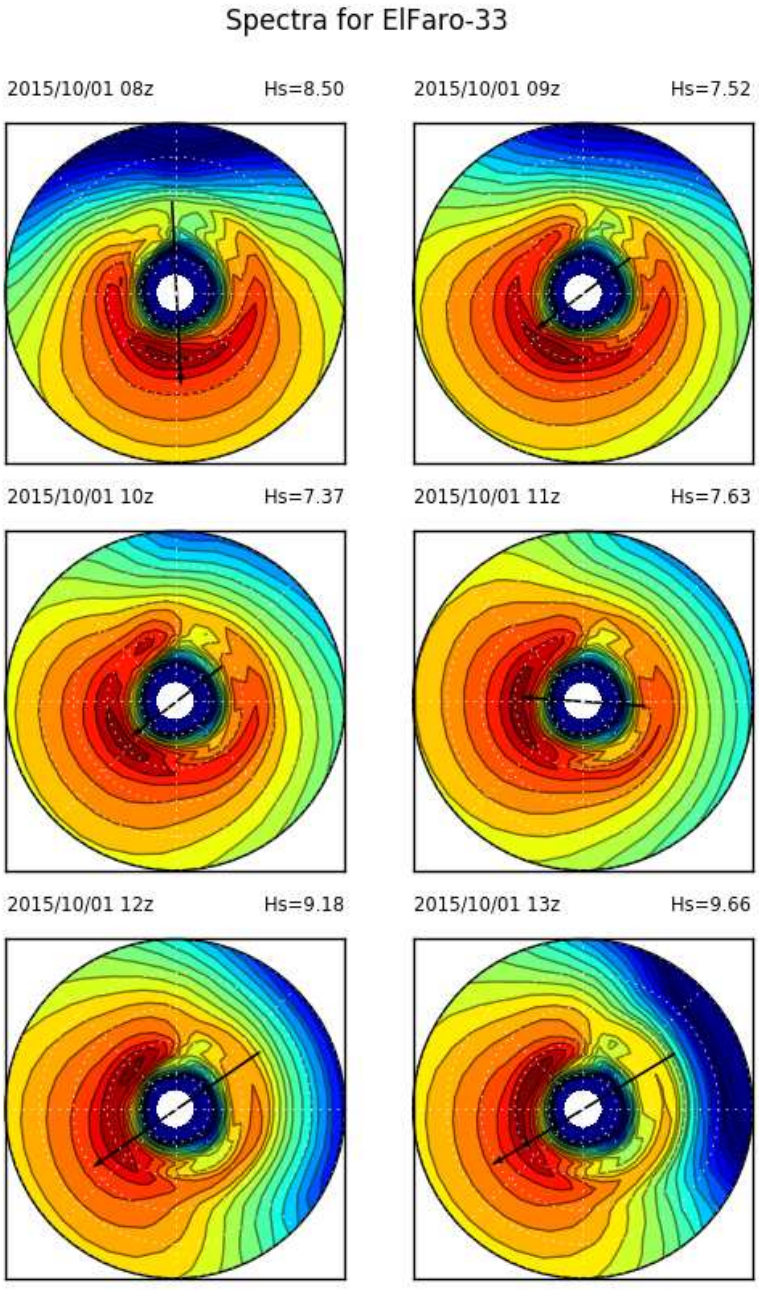

Figure 59: Spectral plot for point ElFaro-33

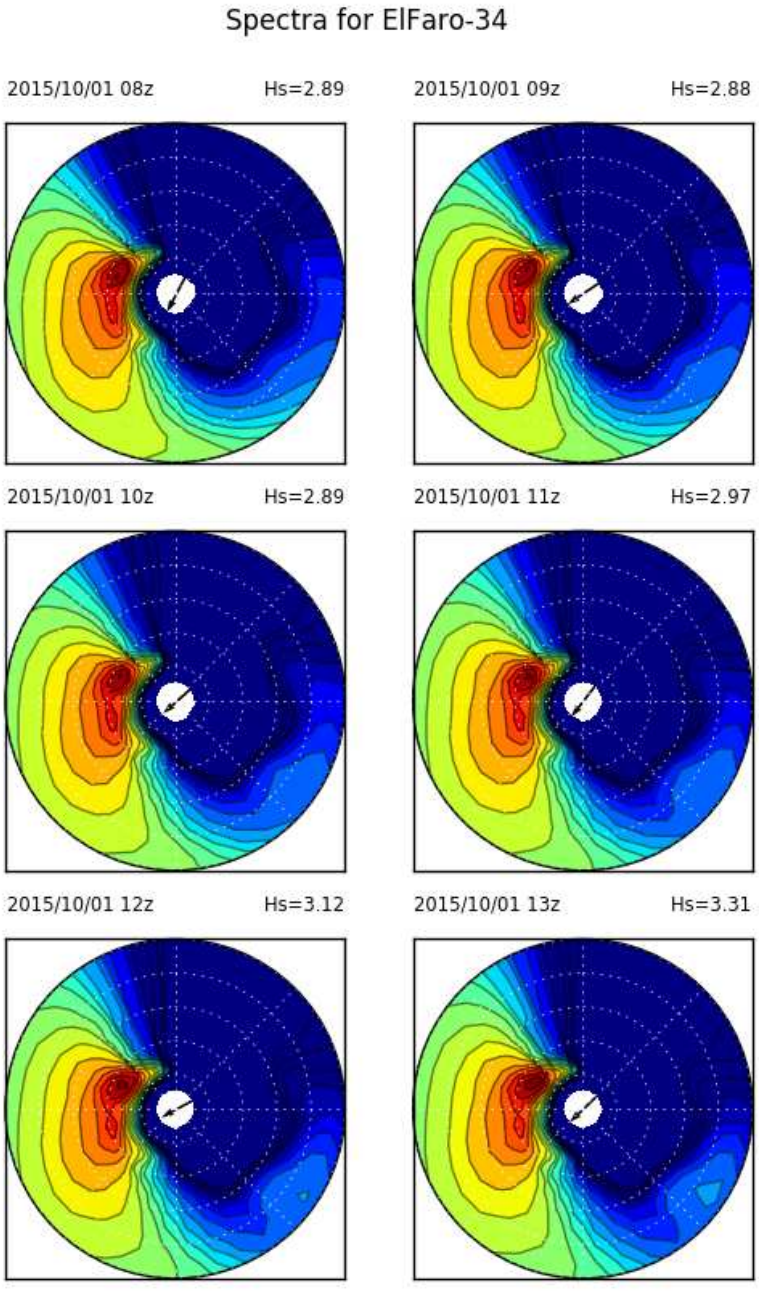

Figure 60: Spectral plot for point ElFaro-34

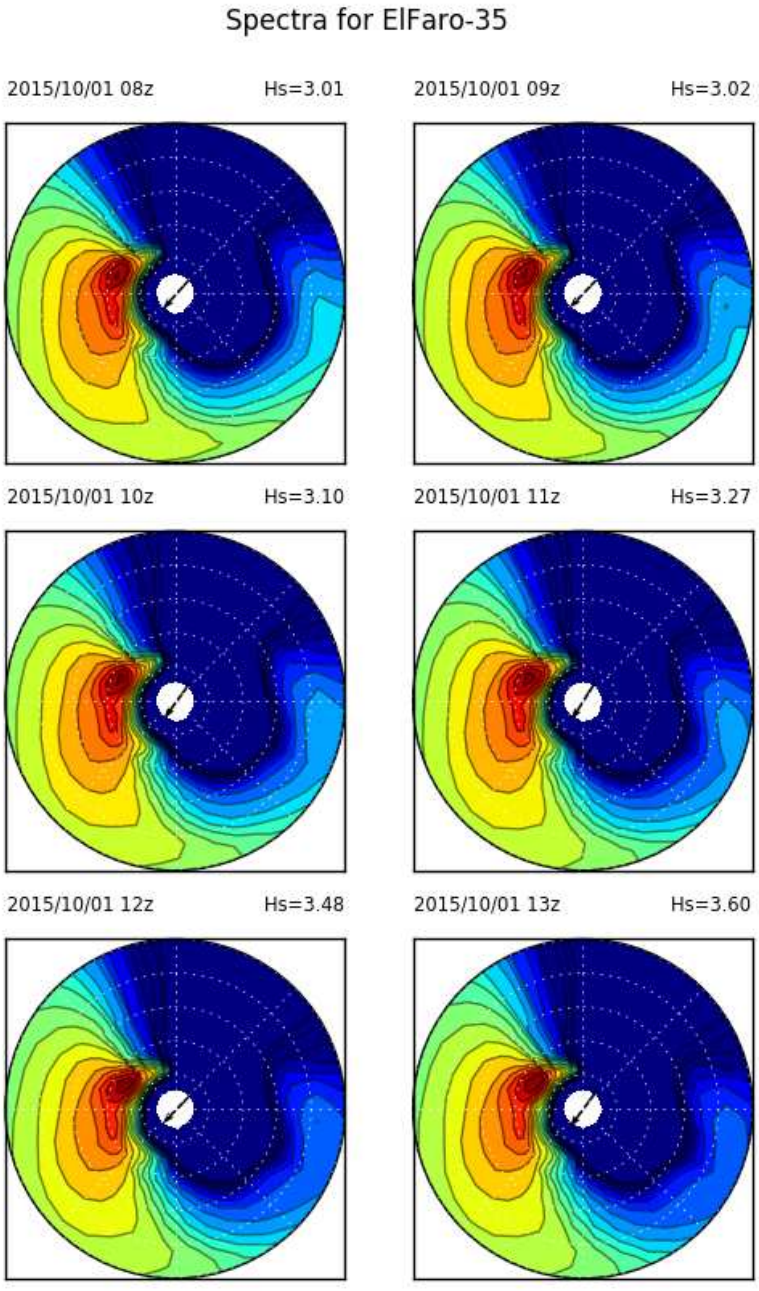

Figure 61: Spectral plot for point ElFaro-35

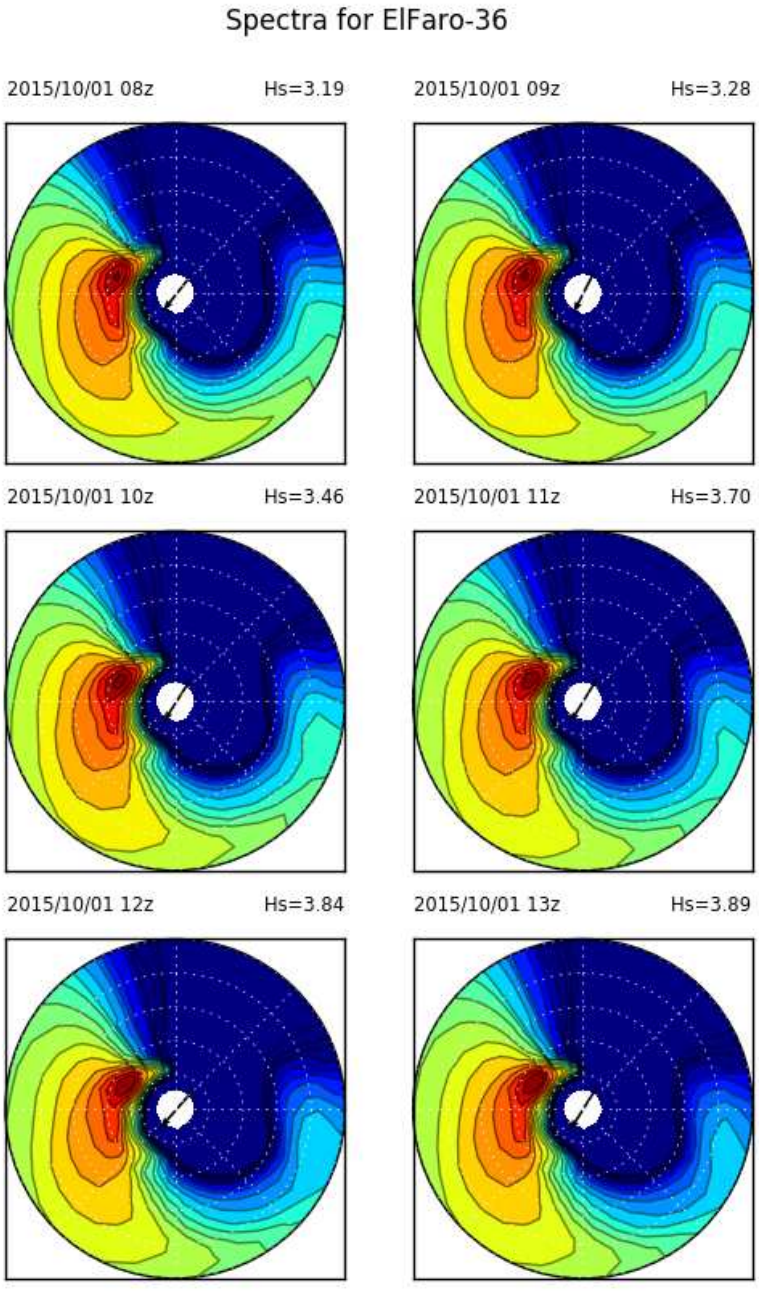

Figure 62: Spectral plot for point ElFaro-36

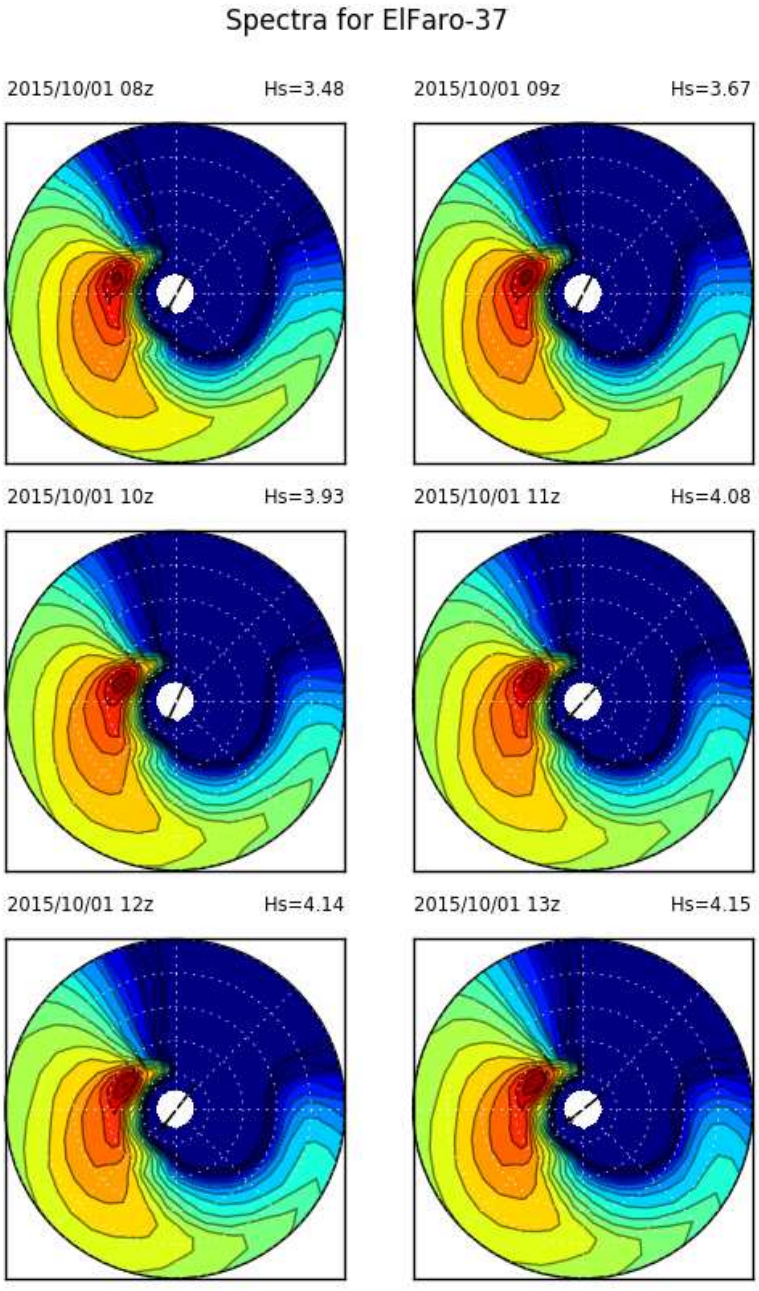

Figure 63: Spectral plot for point ElFaro-37

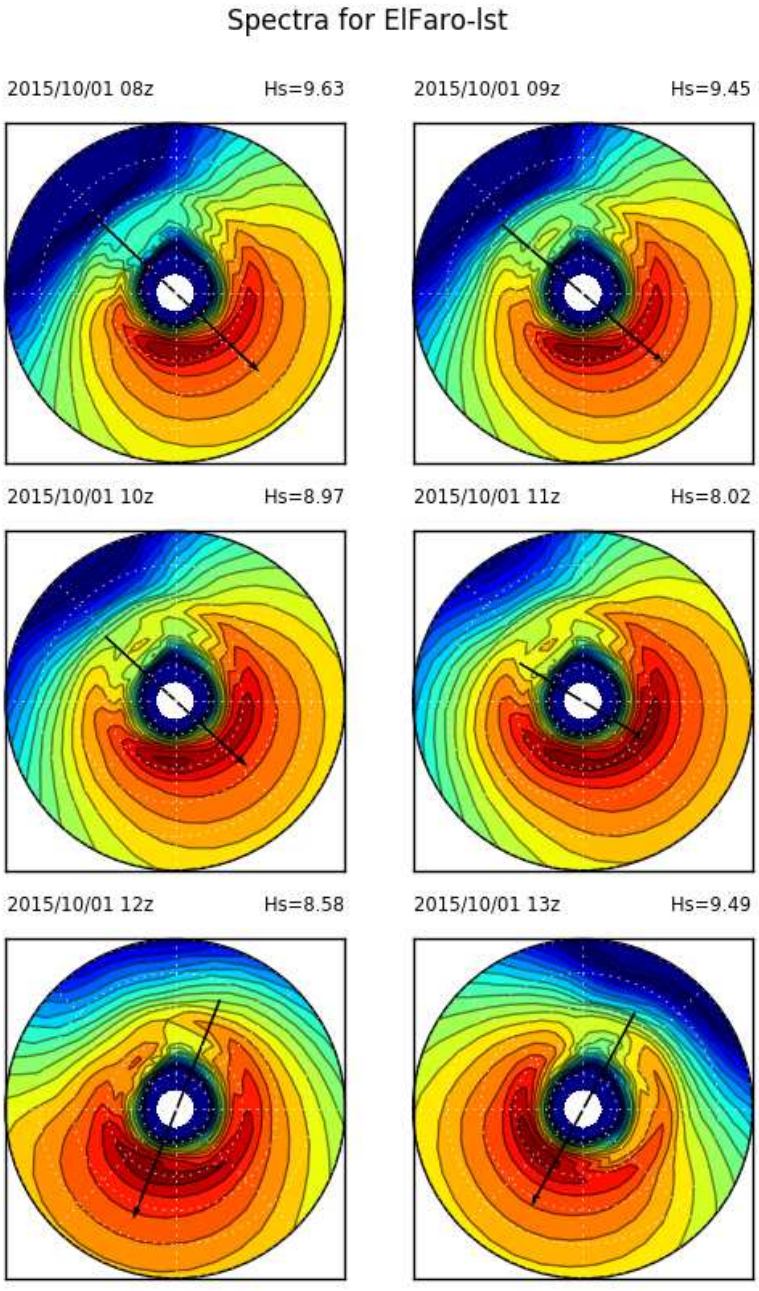

Figure 64: Spectral plot for point ElFaro-lst

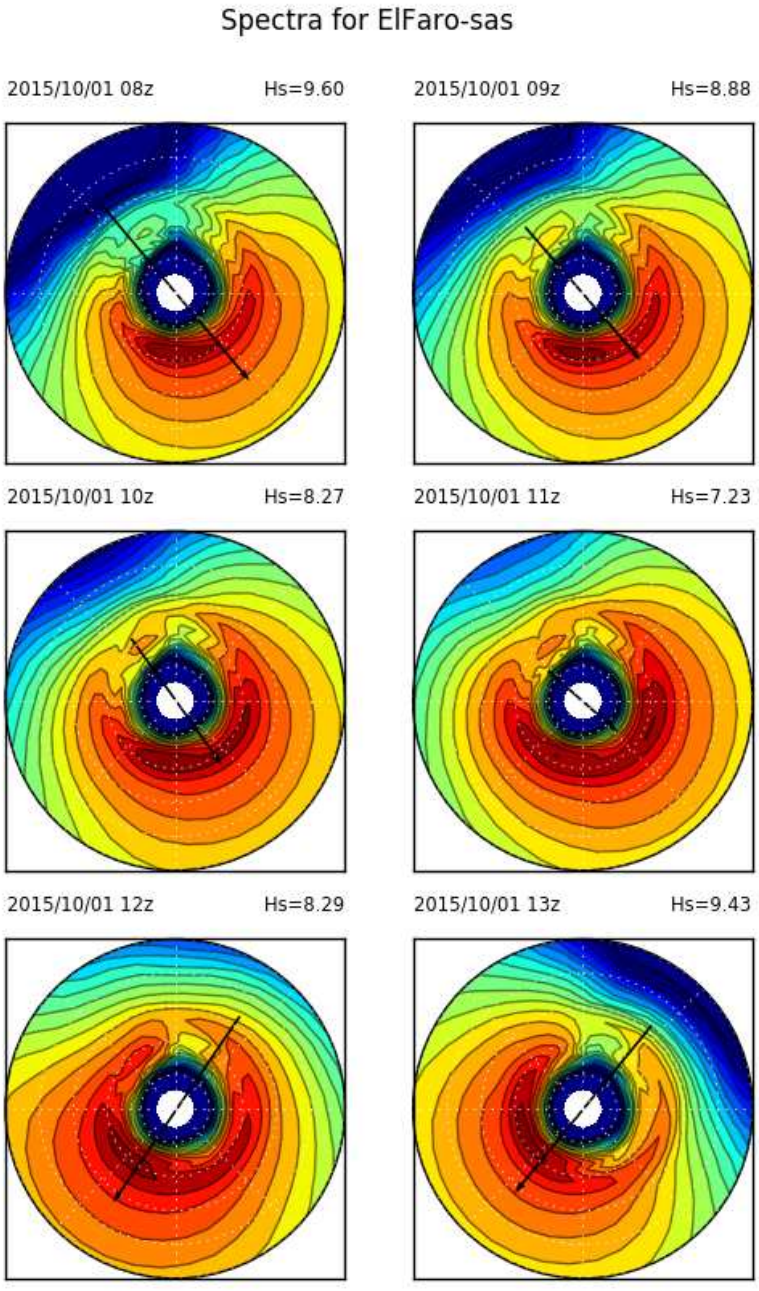

Figure 65: Spectral plot for point ElFaro-sas

B Matlab script for reading a 2D wave spectra file

```
 function b = read_ww3sp(filename)

% M-file to read in data from a 2D spectral file in WW3 V2.22 format
% J. Henrique Alves, March, 2000
% Modified into a function form by A Chawla, June 2011

 if (exist(filename,'file'))
    fid=fopen(filename);
 else
    fprintf(1,'ERROR : File Not found !!');
    return;
 end;

% Scan basic properties of spectra from file
 dum=fscanf(fid,'%c',[23]);
 NF =fscanf(fid,'%g',[1]);
 ND =fscanf(fid,'%g',[1]);
 dum=fscanf(fid,'%s',[1]);
 dum=fscanf(fid,'%c',[33]);
 f=fscanf(fid,'%g',NF);
 dir=fscanf(fid,'%g',ND);
 fprop=f(2)/f(1);
 fdum=[f(1)/fprop;f];
 df=diff(fdum);
 dtheta=abs(dir(2)-dir(1));

 b.f = f;
 b.dir = dir;

 dir(end+1) = dir(1); % Closing for circular integral

% Loop over times
 index = 0;

 b.time = [];
 b.espt = [];
 b.U10 = [];
 b.Udir=[];
 b.cU=[];
```

```
b.cdir=[];
b.sp1d = [];
b.hs = [];
b.dp = [];
b.fp = [];
while ~feof(fid)

   dumdate=fscanf(fid,'%g',2);
   if numel(dumdate)
       year = floor(dumdate(1)/10000);
       month = floor(dumdate(1)/100) - year*100;
       day = dumdate(1) - year*10000 - month*100;
       hr = floor(dumdate(2)/10000);
       mn = floor(dumdate(2)/100) - hr*100;
       sc = dumdate(2) - hr*10000 - mn*100;

       b.time(index+1) = datenum(year,month,day,hr,mn,sc);

       stn=fscanf(fid,'%c',13);
       poslat=fscanf(fid,'%g',1);
       poslon=fscanf(fid,'%g',1);
       depth=fscanf(fid,'%g',1);
       U10=fscanf(fid,'%g',1);
       Udir=fscanf(fid,'%g',1);
       cU = fscanf(fid,'%g',1);
       cdir = fscanf(fid,'%g',1);
       sp2d=fscanf(fid,'%g',[NF,ND]);

       if (index == 0)
           b.name = stn;
           b.lat = poslat;
           b.lon = poslon;
           b.depth = depth;
       end;
       b.U10(index+1) = U10;
       b.Udir(index+1) = Udir;
       b.cU(index+1) = cU;
       b.cdir(index+1) = cdir;

       b.espt{index+1} = sp2d;
       b.sp1d{index+1} = sum(sp2d')*dtheta;
       b.hs(index+1) = 4*sqrt(trapz(f,b.sp1d{index+1}));
```

```
        % Computing peak direction
        sp2d(:,end+1)=sp2d(:,1);
        [tmp,loc]=max(b.sp1d{index+1});
        b1=trapz(dir,sin(dir)'.*sp2d(loc,:));
        a1=trapz(dir,cos(dir)'.*sp2d(loc,:));
        theta_m = atan2(b1,a1);
        if (theta_m < 0)
           theta_m = theta_m + 2*pi;
        end;
        b.dp(index+1) = theta_m;
        b.fp(index+1) = f(loc);

        index = index+1;
    end;
end;

fclose(fid);
return;
```